HIPPOCAMPUS 11:251–274 (2001)

Computational Model of Carbachol-Induced Delta, Theta, and Gamma Oscillations in the Hippocampus

Paul H.E. Tiesinga,[1,2*] Jean-Marc Fellous,[2,3]
Jorge V. José,[4] and Terrence J. Sejnowski[1–3,5]

[1]*Sloan Center for Theoretical Neurobiology, Salk Institute, La Jolla, California*
[2]*Computational Neurobiology Laboratory, Salk Institute, La Jolla, California*
[3]*Howard Hughes Medical Institute, Salk Institute, La Jolla, California*
[4]*Center for Interdisciplinary Research on Complex Systems, and Department of Physics, Northeastern University, Boston, Massachusetts*
[5]*Department of Biology, University of California-San Diego, La Jolla, California*

ABSTRACT: Field potential recordings from the rat hippocampus in vivo contain distinct frequency bands of activity, including δ (0.5–2 Hz), θ (4–12 Hz), and γ (30–80 Hz), that are correlated with the behavioral state of the animal. The cholinergic agonist carbachol (CCH) induces oscillations in the δ (CCH-δ), θ (CCH-θ), and γ (CCH-γ) frequency ranges in the hippocampal slice preparation, eliciting asynchronous CCH-θ, synchronous CCH-δ, and synchronous CCH-θ with increasing CCH concentration (Fellous and Sejnowski, Hippocampus 2000;10:187–197).

In a network model of area CA3, the time scale for CCH-δ corresponded to the decay constant of the gating variable of the calcium-dependent potassium (K-AHP) current, that of CCH-θ to an intrinsic subthreshold membrane potential oscillation of the pyramidal cells, and that of CCH-γ to the decay constant of GABAergic inhibitory synaptic potentials onto the pyramidal cells. In model simulations, the known physiological effects of carbachol on the muscarinic and K-AHP currents, and on the strengths of excitatory postsynaptic potentials, reproduced transitions from asynchronous CCH-θ to CCH-δ and from CCH-δ to synchronous CCH-θ. The simulations also exhibited the interspersed CCH-γ/CCH-δ and CCH-γ/CCH-θ that were observed in experiments. The model, in addition, predicted an oscillatory state with all three frequency bands present, which has not yet been observed experimentally. *Hippocampus 2001;11:251–274.* © 2001 Wiley-Liss, Inc.

KEY WORDS: acetylcholine; synchronization; neuromodulation; noise; subthreshold oscillations

INTRODUCTION

The human electroencephalogram (EEG) contains multiple synchronous rhythms that reflect spatially and temporally ordered activity (Basar et al., 1999; Glass and Riding, 1999). Delta rhythms (0.5–2 Hz) are involved in signal detection and decision making (Basar-Eroglu et al., 1992); theta oscillations (4–12 Hz) are related to cognitive processing and cortico-hippocampal interactions (Vinogradova, 1995); and gamma oscillations (30–80 Hz) can be found in a variety of structures under different behavioral conditions (Basar et al., 1999; Ritz and Sejnowski, 1997; Singer and Gray, 1995). Human performance during an alterness task can be predicted by the correlated increase or decrease of gamma and theta band activity (Makeig and Jung, 1996). The neural mechanisms for these correlated changes in EEG frequency content are unknown, but they are likely to involve the activity of neuromodulatory centers (McCormick, 1992; Stewart and Fox, 1990; Leung, 1998). For instance, in vivo microdialysis studies in cats show that the level of acetylcholine in the cortex and hippocampus is reduced during delta oscillations, and can be up to four times higher during theta activity (Marrosu et al., 1995).

Recordings from the hippocampus reveal oscillations in the delta, theta, and gamma ranges, depending on behavioral conditions (reviewed by Fellous and Sejnowski, 2000). The amplitude and frequency of hippocampal theta and gamma rhythms are correlated in anesthetized rats, indicating that the underlying neural mechanisms are not independent (Bragin et al., 1995). Furthermore, a subpopulation of hippocampal cells either discharges at low frequency or in the theta-frequency range, depending on level of cholinergic innervation of the hippocampus (Bland and Colom, 1993; Steriade et al., 1993). The theta rhythm in vivo is thought to depend on the cholinergic and GABAergic septal inputs (Brazh-

Grant Sponsor: Sloan Foundation; Grant Sponsor: Howard Hughes Medical Institute.
* Correspondence to: Paul Tiesinga, Sloan Center for Theoretical Neurobiology, Salk Institute, 10010 N. Torrey Pines Road, La Jolla, CA 92037.
E-mail: tiesinga@salk.edu
Accepted for publication 12 October 2000

nik and Fox, 1997; Freund and Antal, 1988; Frotscher and Leranth, 1985; Stewart and Fox, 1990). The frequency of the theta rhythm is controlled by GABAergic phasic inputs from the septum, while its power is controlled by septal cholinergic afferents (Brazhnik et al., 1993; Lee et al., 1994; Soltesz and Deschenes, 1993; Stewart and Fox, 1990; Ylinen et al., 1995). These mechanisms are difficult to study experimentally because they involve two interacting structures and two interacting transmitter systems.

The in vitro hippocampal preparation provides a simplified framework in which the mechanisms underlying theta, delta, and gamma rhythms, and the transitions between the rhythms, can be studied in the absence of input from the septum. Furthermore, recent experiments indicate that the intrinsic properties of the isolated CA3 region in the hippocampus contribute to theta rhythms observed in vivo (Kocsis et al., 1999). Muscarinic activation of the CA3 region, using the agonist carbachol, results in synchronous population activity in the delta (Boguszewicz et al., 1996; Fellous and Sejnowski, 2000), theta (Bland et al., 1988; Fellous and Sejnowski, 2000; Konopacki et al., 1987; MacVicar and Tse, 1989; Williams and Kauer, 1997), and gamma (Fellous and Sejnowski, 2000; Fisahn et al., 1998) bands. These intracellular studies have shown that cholinergically induced delta and theta (CCH-δ and CCH-θ) oscillations depended on the pyramidal cell network of the CA3 region, but gamma (CCH-γ) also required an intact network of GABAergic interneurons. The level of activation of cholinergic receptors in the slice determines which of the three oscillations will occur or predominate (Fellous and Sejnowski, 2000).

The biophysical effects of carbachol have been studied extensively. Carbachol blocks several potassium conductances, including $I_{K\text{-}AHP}$, and I_M in a concentration-dependent manner (Madison et al., 1987; McCormick, 1989). This depolarizes the pyramidal cells, unmasking subthreshold membrane potential oscillations in the theta-frequency range (Leung and Yim, 1991; Fellous and Sejnowski, 2000). In addition, carbachol reduces the average strength of excitatory postsynaptic potentials (EPSPs) and changes their distribution (Hasselmo, 1995; Hasselmo et al., 1995; Patil and Hasselmo, 1999).

Several investigators have studied the mechanisms underlying delta- (Traub and Miles, 1991), theta- (Traub et al., 1992), and gamma-frequency range oscillations (Wang and Buzsáki, 1996) in isolation. The biophysical effects of carbachol on single-cell dynamics have been investigated in detailed models (Menschik and Finkel, 1998, 1999). However, there are no hypotheses for how the level of cholinergic activation triggers and controls the transitions between these oscillations.

The goal of this study was to determine under what conditions, and by what mechanisms, the hippocampal area CA3 can support the CCH-δ, CCH-θ, and CCH-γ oscillations, using a combined experimental and modeling approach. In particular, we investigated how carbachol induced transitions between these states in a concentration-dependent manner. Because carbachol changes the intrinsic neuronal dynamics and network dynamics, it has proven difficult to dissect these two contributions solely by experimental methods. Computer simulations were used to disentangle these two contributions and suggest further experiments.

METHODS

Experimental Methods

All experiments were carried out in accordance with animal protocols approved by the NIH. Young (20–30 days) Sprague-Dawley rats were anesthetized using metofane and decapitated, and their brains were quickly removed in cold artificial cerebrospinal fluid (ACSF). After free-hand razor cuts, brains were placed on a vibratome (series 1000), and 400-μm transversal hippocampal slices were obtained. Slices were held in ACSF in mM: NaCl, 124; NaH_2CO_3, 26; D-glucose, 10; KCl, 5; $CaCl_2$, 2; $MgSO_4$, 2; and NaH_2PO_4, 1.2, saturated with 95% O_2/5% CO_2, at room temperature. Slices were then placed in the recording chamber, at 31–32°C and perfused at constant flow (2–3 ml/min). Field recordings were obtained with glass microelectrodes (ACSF filled, 300–400 KΩ) pulled using a Flaming/Brown micropipette puller (P97, Sutter Instruments) and placed in the cell body layer in CA3. Whole-cell patch-clamp recordings were achieved using glass electrodes (4–10 MΩ, containing in mM: $KmeSO_4$, 140; Hepes, 10; NaCl, 4; EGTA, 0.1; Mg-ATP, 4; Mg-GTP, 0.3; phosphocreatine 14). Patch-clamp was performed under difference interference contrast visual control. In most experiments, Lucifer yellow (RBI, 0.4%) was added to the internal solution. At the end of each experiment, high-intensity mercury arc light was shone on the cell, and fluorescence was recorded on videotape. Cells were characterized on the basis of their morphology and physiological responses to square pulses. All drugs were obtained from R.B.I. or Sigma, freshly prepared in ACSF, and bath-applied. Data were acquired with Labview 5.0 and a PCI-16-E1 data acquisition board (National Instrument), and analyzed with MATLAB (The Mathworks) and Excel (Microsoft). Further details can be found in Fellous and Sejnowski (2000).

Simulation Methods

The pyramidal cell model was based on the Pinsky-Rinzel (PR) model (Pinsky and Rinzel, 1994). It consisted of two compartments, the soma and the dendrite. The soma contained the delayed-rectifier potassium, $I_{K\text{-}DR}$, the fast sodium, I_{Na}, and a leak current, I_L. The dendrite contained the slower currents, specifically, the calcium, I_{Ca}, the calcium-dependent potassium current responsible for the slow afterhyperpolarization (AHP), $I_{K\text{-}AHP}$, and another calcium-dependent potassium current, $I_{K\text{-}C}$, in addition to the leak current. The compartments were electrically connected via a conductance g_c. This model reproduces the salient features of a more detailed model of a CA3 pyramidal neuron by Traub et al. (1991). See the Appendix for details.

A number of changes were made to the Pinsky-Rinzel model. A muscarinic current I_M was added to the dendritic compartment. The kinetics were taken from Warman et al. (1994). Persistent-like sodium and potassium currents, I_{NaO} and I_{KO}, respectively, were also included. The kinetics were chosen so that these currents were activated close to resting membrane potential, and could generate the subthreshold theta-frequency membrane potential oscillations. We further tuned the model so that it reproduced our experimental

TABLE 1.

Parameter Values for Pyramidal Cell Model for Low (2–4 μM), Medium (4–13 μM), and High (13–40 μM) Carbachol Concentrations

CCH (μM)	g_{Ca} (mS/cm^2)	g_{K-AHP} (mS/cm^2)	g_M (mS/cm^2)	I_{app} (μA/cm^2)
2–4	10	0.8	0.3–0.4	0.15
4–13	10	0.8	0.2–0.3	0.27
13–40	6	0.2	0.0–0.0	0.0–1.35

observations (Fellous and Sejnowski, 2000; Fellous et al., 1999), and those reported earlier (Leung and Yim, 1991). In particular, 1) the membrane potential oscillations depended on a sodium and a (TEA-sensitive) potassium current; 2) the membrane potential oscillations were induced by a depolarization, and the frequency of the oscillations increased with additional depolarization; 3) neurons produced single spikes instead of bursts; and 4) neurons only fired on some cycles of the theta-frequency membrane potential oscillation.

The effects of carbachol on the intrinsic dynamics were mediated by $I_{K\text{-}AHP}$, I_M, I_{Ca}, and I_{app}. $I_{K\text{-}C}$ is not sensitive to carbachol (Madison et al., 1987) and was not modified in the simulations. For clarity, three ranges of carbachol concentrations were examined: low, medium and high (see Table 1). These three parameter sets take into account the following salient experimental results (Madison et al., 1987): first, I_M was 10% inhibited at 1 μM CCH, and 80% at 10 μM CCH. Its largest change thus occurred between 1–13 μM CCH. Second, at 1 μM CCH, $I_{K\text{-}AHP}$ was already 70% inhibited from its 0 μM CCH value. It was reduced further (but more slowly compared to I_M) to 95% inhibition at 10 μM CCH. In the model its strength was reduced to 1/4 of its 1 μM value for concentrations above 13 μM CCH as in (Traub et al., 1992). Third, the driving current was increased (yielding effects similar to decreasing g_L) to account for the additional depolarization. The calcium current was also reduced with increasing CCH concentration (Menschik and Finkel, 1998, 1999). The concentration-dependent effects of carbachol used here were measured for pyramidal cells in region CA1 (Madison et al., 1987). Here we assume, as in previous works (Traub et al., 1992; Menschik and Finkel, 1998, 1999), that the currents of CA3 pyramidal cells are modulated by carbachol in a quantitatively similar way.

The interneuron model consisted of one compartment with a sodium, I_{Na}, a potassium, I_K, and a leak current (Wang and Buzsáki, 1996). The kinetics of the currents were different from those in pyramidal cells (see Appendix). Because no detailed biophysical data were available, the excitatory effect of carbachol was mimicked by increasing a constant depolarizing current.

Interneurons projected via $GABA_A$ synapses to pyramidal cells, and to other interneurons. The pyramidal cells projected via AMPA synapses to other pyramidal cells and to interneurons (see Appendix for details). The specific network architecture is shown in the figures themselves. We did not include NMDA or $GABA_B$ receptors in the model. Experimental evidence indicates that these conductances do not significantly affect the oscillations observed in our hippocampal preparation (Fellous and Sejnowski, 2000). The synaptic connections were chosen with probability $P(\text{neuron}_i \rightarrow \text{neuron}_j)$ for each pair of neurons, and each instantiated synapse had equal strength (see Appendix). The connection probability of the recurrent excitatory synapses were chosen in a similar range compared to Traub et al. (1992), where $P \sim 0.02$. We increased the probability to $P = 0.1\text{–}0.5$, to account for the smaller number of neurons used in our simulations (50–500 vs. ≥1,000 in Traub et al., 1992). For the mutual inhibitory connections between interneurons, we used all-to-all connectivity as in previous studies (Wang and Buzsáki, 1996; White et al., 1998a; Tiesinga and José, 2000a). The connection probabilities between interneurons and pyramidal cells were considered free parameters and were varied between simulations. The actual connection probabilities and synaptic conductances used in our simulations are listed in the corresponding figure captions only.

Carbachol modulates the strength of the recurrent excitatory synaptic connections. Experimental data for CA1 show that the strengths of Schaffer collateral synapses are reduced by about 50% at 10 μM CCH, whereas the perforant path synapses were affected to a lesser extent (Hasselmo and Schnell, 1994). The strengths of the Schaffer collateral field EPSPs were reduced to an even larger extent (Sheridan and Sutor, 1990). In our model, synaptic strength was taken to be constant for the low and medium carbachol concentrations (CCH <13 μM), and reduced by 50% for high carbachol concentrations (CCH >13 μM). We also studied in some simulations the effect of reducing synaptic strength for CCH <13 μM. We did not model the effects of carbachol on the strength of inhibitory connections.

The model neurons had different time scales, which could potentially lead to numerical instabilities. A fourth-order Runge-Kutta algorithm was used for the time-integration in the network simulations (Press et al., 1992). Using the same time step, $dt = 0.05$ ms, as in Pinsky and Rinzel (1994), we reproduced Figures 3 and 5 of Pinsky and Rinzel (1994) (not shown). Good agreement was also obtained with the PR model implemented in the standard simulation package NEURON (Hines and Carnevale, 1997), and with an adaptive stepsize Runge-Kutta algorithm (Press et al., 1992).

For certain parameter settings, the dynamics of the Pinsky-Rinzel model neuron displayed signs of chaos (Pinsky and Rinzel, 1994). We did not observe chaos in our simulations.

We also studied the dynamics of a single pyramidal cell driven by a simulated presynaptic spike train that represented the inputs of many different neurons. The input spike train was generated as a Poisson process with a constant firing rate f_{EPSP} (see, for instance, Rieke et al., 1997; Press et al., 1992). Briefly, we discretized time in bins of $\Delta t = 0.01$ ms. The probability of a spike in a given bin was then $f_{EPSP}\Delta t$. We drew a random number ξ, uniformly distributed between zero and one; when $\xi \leq f_{EPSP}\Delta t$, a presynaptic spike was generated. Each presynaptic spike generated an exponentially decaying conductance pulse with the same time constant, 2 ms, as an AMPA synapse in the network simulation. In some cases cases we generated a spike train with a time-varying firing rate (for details see Tiesinga and José, 2000a).

Initial conditions could be crucial, so for the pyramidal cells, initial values for the voltage (the same for both compartments) and gating variable q (or equivalently, the initial calcium concentration) were carefully chosen. In most simulations, the voltage was set to -64.2 mV and q was chosen from a uniform distribution between zero and an upper range varying between between 0.01–0.20. For interneurons, the voltage was either set to -65 mV, or uniformly distributed between -75 and -55 mV. The other gating variables were set at their steady-state values.

Calculated Quantities and Units

The spike times, determined during simulation runs, were the times at which the somatic voltage crossed -30 mV (0 mV for interneurons) from below, i.e., $V(t - dt) < -30 \text{ mV} \leq V(t)$. We chose the threshold at -30 mV to detect all the spikes during a burst of the pyramidal cell. The power spectrum $|V(f)|^2$ of the voltage was computed using the psd routine, and the transfer function $S = \langle V(f)I(f)\rangle / \sqrt{\langle |V(f)|^2\rangle}$ using the tfe routine, in MATLAB. The parameter n_{fft} used in these routines was either 4,096 or 8,192.

In the rastergrams, each solid circle represents one spike. Its x-coordinate is the spike time, and its y-coordinate is the neuron's index. The time-dependent firing rate of the network was calculated by supplying all the spike times to the MATLAB routine hist with bin widths 1 (CCH-γ), 5 (CCH-θ), or 20 ms (CCH-δ and asynchronous CCH-θ).

All quantities were normalized by the surface area of the neuron. This leads to the following system of units: the membrane potential V in mV, time t in ms, firing rate f in Hz, membrane capacitance C_m in μF/cm^2, conductance g_x in mS/cm^2, voltage noise ξ in mV/ms, strength of neuroelectric noise D in mV^2/ms, the rate constants α_x and β_x in ms^{-1}, and the current I in μA/cm^2. The gating variables and the time-scale ϕ are dimensionless. All results are expressed in this system of units.

RESULTS: NETWORK OF PYRAMIDAL CELLS

Low Carbachol Concentrations Induce Subthreshold Oscillations

Some excitatory cells in the hippocampus, enthorhinal cortex, neocortex, and other brain areas display subthreshold membrane oscillations (Alonso and Llinas, 1989; Llinas et al., 1991; Leung and Yim, 1991). Low concentrations of carbachol can induce subthreshold membrane oscillations in the theta-frequency range (Fellous and Sejnowski, 2000). Subthreshold oscillations are also observed during depolarization of the neuron by current injection (Leung and Yim, 1991; Fellous et al., 1999). These effects were reproduced in the model of a hippocampal pyramidal neuron (see Methods).

Figure 1a illustrates the dynamics of the neuron model driven by a simulated spike train (see Methods) of excitatory postsynaptic potentials (EPSPs). The muscarinic potassium current and the synaptic strength were progressively decreased from curve 1 to 3, while the number f_{EPSP} of impinging EPSPs was increased. At first the membrane potential was noisy, and the subthreshold oscillation was barely visible (Fig. 1a, curve 1). Then waxing and waning subthreshold oscillations in the theta-frequency range became visible (Fig. 1a, curve 2). Infrequently an action potential was present at the peak of the oscillations. Finally, more spikes were present (Fig. 1a, curve 3). The pyramidal cell model in Figure 1 is based on the model of Traub et al. (1991). However, in the Traub model the neuron bursts for small driving currents (Traub et al., 1991; Pinsky and Rinzel, 1994), whereas here the model neuron produces single spikes.

In Figure 1b, the intracellular membrane potential from a pyramidal cell in a hippocampal slice is shown during the 2 μM CCH wash-in. The number of spontaneous EPSPs and the membrane potential increase, whereas the muscarinic potassium current decreases. The simulations resembled the experimental recording. A similar increase in oscillation amplitude leading to spikes can also be produced in the model by changing other parameters, such as increasing the driving current, reducing the muscarinic potassium conductance, or increasing the presynaptic EPSP frequency (not shown). The above results were obtained using a presynaptic spike train with a constant firing rate, but injected white noise currents can induce the oscillations as well. We also applied a periodic synaptic drive corresponding to an ensemble of neurons synchronized at the theta-frequency range. In that case, more action potentials were generated for the same synaptic strength and average presynaptic firing rate (not shown). A similar resonance to a theta-frequency current drive was also observed in experiments (Fellous et al., 1999).

Subthreshold membrane oscillations can be characterized using a transfer function (Hutcheon et al., 1996a,b; Lampl and Yarom, 1997; Leung and Yu, 1998). The transfer function $S(f)$ describes the attenuation of a particular frequency component f of the input. It is the ratio of the Fourier transforms of the output and input (Arfken and Weber, 1995). Here we calculate it for noisy data as the crosscorrelation of the input current with the resulting membrane potentials divided by the spectrum of the input current (see Methods). In Figure 1c, the transfer function shown on top was obtained from a 15-s-long voltage trace without any action potentials. The square root of the power spectrum of spontaneous subthreshold activity measured in experiment was included below. If the experimental noise spectrum is flat, the power spectrum is identical to the transfer function up to a normalization constant. The transfer function had a well-defined peak around 6 Hz, within the theta-frequency range. For high frequencies, $f > 10$ Hz, it decayed as $1/f$. The transfer function of a neuron without a resonance has a maximum at zero frequency and can be described as a low-pass filter. There were significant statistical fluctuations in the low- and high-frequency domains due to the stochastic character of the spike train input.

The transfer function can also be determined by driving the neuron with pure sinusoidal currents. The transfer function is proportional to the amplitude of the resulting voltage oscillation at frequency f. For purely linear systems, both methods yield the same result, but the latter method is less noisy. The resulting graphs are

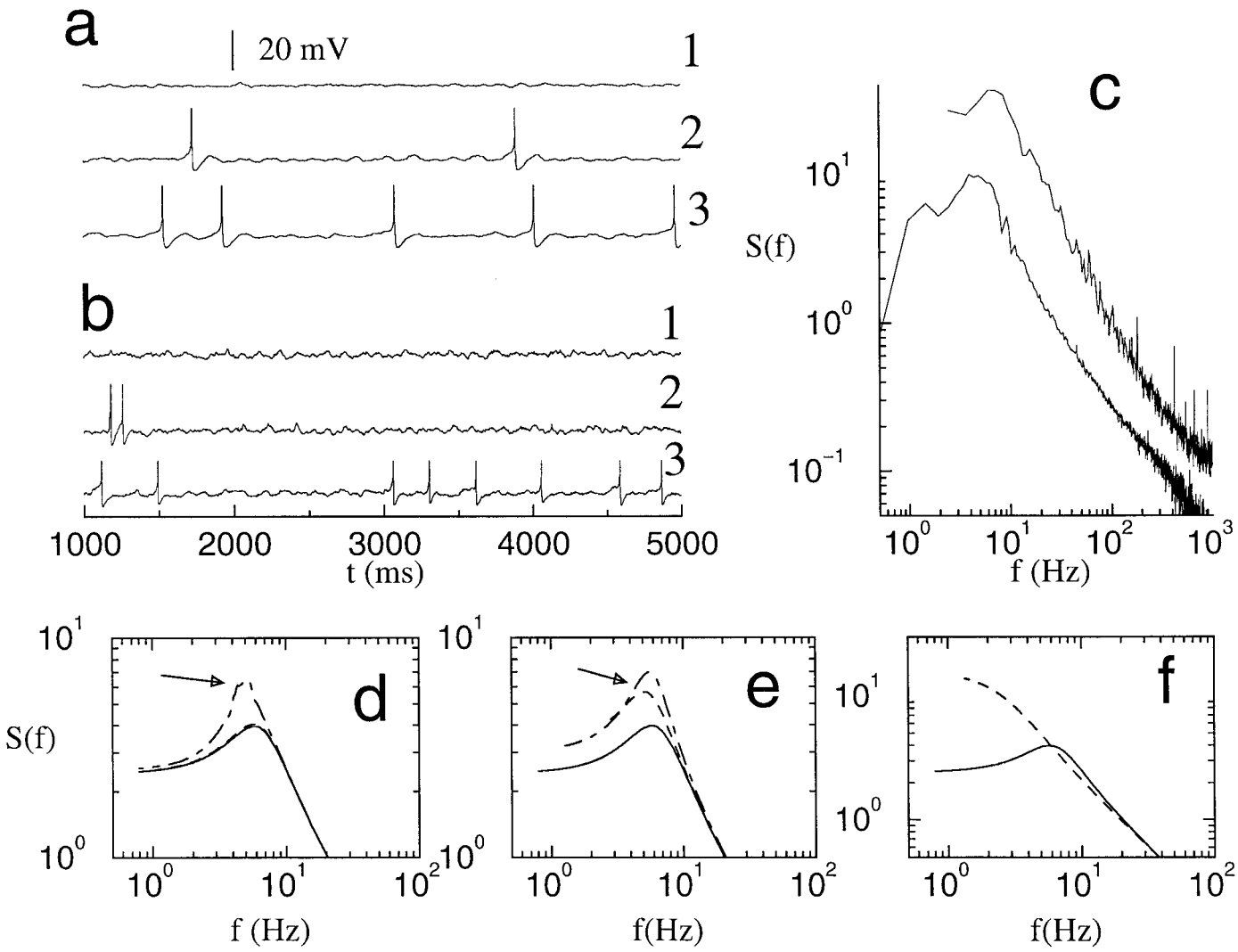

FIGURE 1. Carbachol-induced depolarization and reduction of muscarinic potassium conductance introduced subthreshold membrane oscillations in a model pyramidal cell. a: Voltage traces of a model neuron driven by a Poisson spike train with a total presynaptic firing rate f_{EPSP}, unitary synaptic conductance g_{AMPA}, and muscarinic potassium conductance g_M. These parameters are changed to mimick the effects of increasing the CCH concentration, (f_{EPSP}, g_{AMPA}, g_M) = (500, 0.004, 0.4) (trace 1), (1200, 0.003, 0.3) (trace 2), and (1630, 0.002, 0.2) (trace 3). b: Experimental intracellular recordings of a pyramidal neuron in CA3 at different times (1, 2, and 3) during 2-μM carbachol wash-in. c: Top trace. Square root of the power spectrum of intracellular voltage recording (multiplied by 2 for clarity), 160,000 pts at a sampling rate of 10 kHz, using Welsh periodograms with n_{fft} = 8,192. Bottom trace. The transfer function $S(f)$, calculated from a model voltage trace of 30,000 points at 2 kHz using n_{fft} = 4,096. Parameters (f_{EPSP}, g_{AMPA}, g_M) = (500, 0.008, 0.4). The voltage trace did not contain any action potentials. d–f: $S(f)$ calculated using sinusoidal input currents of frequency f (see text). d: We vary the amplitude of the sinusoidal current, A = 0.01 (solid line), 0.2 (dashed line), and 0.5 (dot-dashed line) with I_{app} = 0.15 and g_M = 0.4. We compare the reference case, A = 0.01, to (e) a reduced muscarinic conductance g_M = 0.2 (dashed line) and an increased current I_{app} = 0.4 (dot-dashed line). f: Spectrum of a model without the I_{NaO} and I_{KO} currents (dashed line). Conductances in mS/cm^2, currents in μA/cm^2.

shown in Figure 1d–f. Results based on a variety of parameter sets were compared to those from the reference set (amplitude A of the sinusoidal current equal to 0.01 μA/cm^2, continuous line in Fig. 1d–f). For amplitudes up to 0.2 μA/cm^2 the membrane behaved in a linear fashion, and the transfer functions fell on top of each other (Fig. 1d). For higher amplitudes, A = 0.5 μA/cm^2, the response became nonlinear. The resonance peak was shifted to lower frequencies and attained a higher value (Fig. 1d, arrow). At theta frequencies the injected current produced action potentials (not shown). (Note that the spectrum in Fig. 1c is different from those shown in Fig. 1d. Synaptic potentials can induce nonlinear effects, in addition to increasing the membrane conductance and generating an average depolarization.) Figure 1e,f was in the linear regime, A = 0.01 μA/cm^2. Decreasing the muscarinic potassium conductance, or depolarizing the neuron via an increased external current, led to an enhanced resonance (Fig. 1e, arrow), consistent with experiments in which carbachol induced a depolarization, and also reduced the muscarinic potassium current. These simulations therefore reproduced subthreshold oscillations induced and enhanced by carbachol.

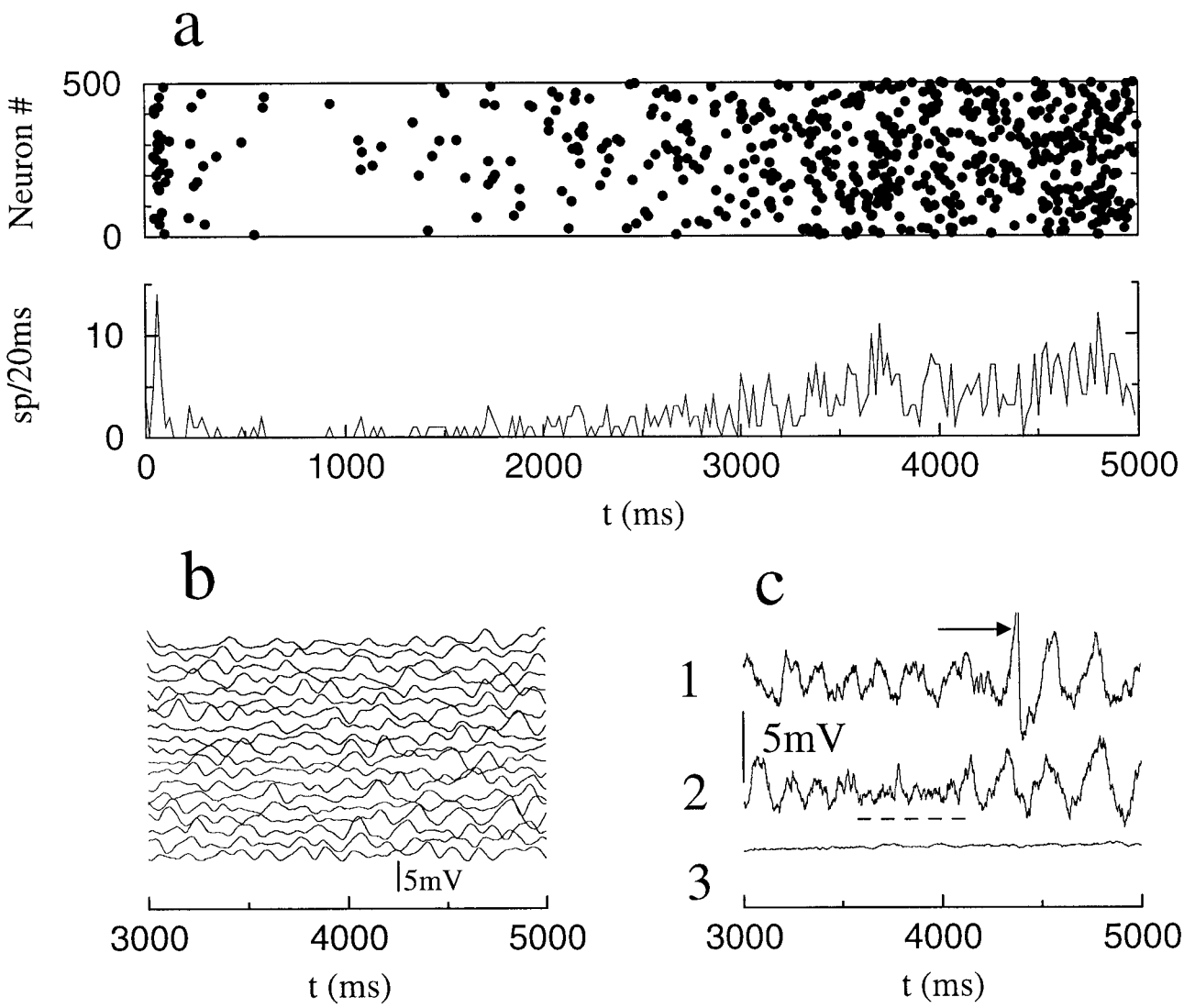

FIGURE 2. Simulations of incoherent CCH-θ oscillations, which were stable against recurrent excitation at low CCH concentration (2 − 4 μM). a: Rastergram (top), and the corresponding firing rate histogram with 20-ms bins (bottom). In the rastergram, the y-ordinate of each circle is given by the neuron index, and the x-ordinate by the spike time. b: Smoothed voltage traces of 20 neurons that did not spike during the last 2,000 ms. c: Two voltage traces (curves 1 and 2). Arrow indicates an action potential. Dashed bar marks waning of subthreshold oscillation. Bottom curve (3) is the average voltage of all the neurons that did not spike during that period. Parameters: N = 500 pyramidal cells, $P(e \rightarrow e)$ = 0.10, g_{AMPA} = 0.003, I_{app} = 0.27, and (g_M, $g_{K\text{-}AHP}$, g_{Ca}) = (0.3, 0.8, 10.0). Conductances in mS/cm^2, currents in μA/cm^2.

When the I_{NaO} and I_{KO} currents responsible for the subthreshold oscillations were also removed, a low-pass filter spectrum was obtained, as expected (dashed line in Fig. 1f).

Incoherent Oscillations in the Theta-Frequency Range

The field potential observed in slice preparations was noisy and asynchronous for low carbachol concentrations of 2–4 μM (Fellous and Sejnowski, 2000). However, the intracellular recordings showed subthreshold oscillations in the theta-frequency range, with infrequent spikes at the peaks of depolarization (Leung and Yim, 1991). Numerical model calculations reproduced this network state (Fig. 2).

The network consisted of 500 pyramidal cells connected by recurrent fast excitatory AMPA synapses. The conductance values were set corresponding to the 2–4 μM CCH range listed in Table 1. After a transient of about 2,000 ms, the network activity slowly increased, and settled in a low firing rate steady state (Fig. 2). Each neuron only fired one or two spikes during the last 2,000 ms of the simulation. There were no signs of synchronized neuronal discharge present in the firing rate histogram. Correlations between neurons were also studied. In voltage traces of 20 neurons that did not spike (Fig. 2b), the subthreshold oscillations were clearly visible, but there was no phase relationship between pairs of neurons. The average membrane potential of all the neurons that did not spike in the last 2,000 ms of the simulation was flat (Fig. 2c3).

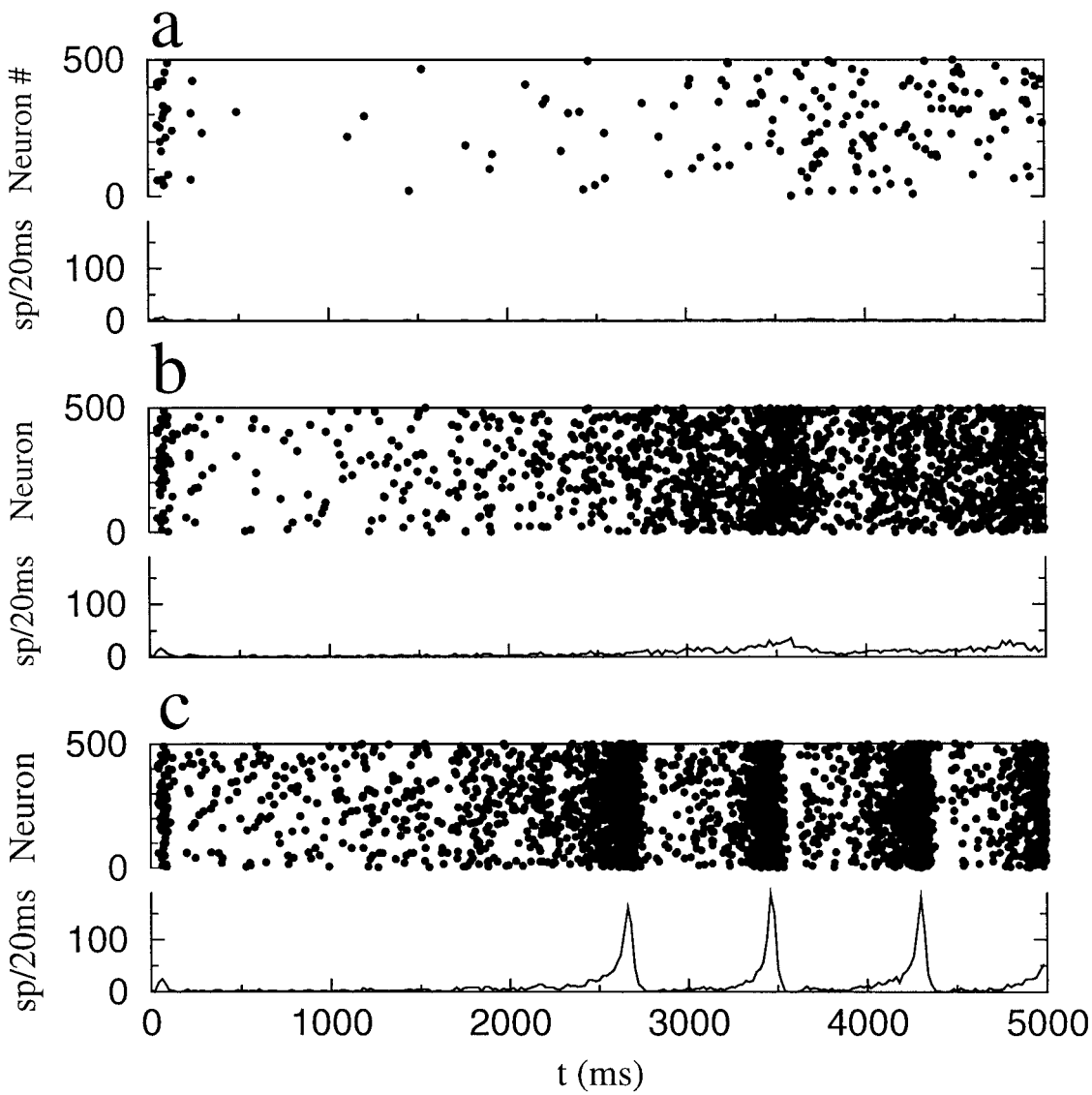

FIGURE 3. Simulations of carbachol-mediated reduction in muscarinic potassium conductance, which destabilized the asynchronous CCH-θ for medium concentrations of CCH (4–13 μM). a–c show the rastergram (top), and the firing rate histogram (bottom, bin width 20 ms). From top to bottom the muscarinic conductance was g_M = 0.35 (a), 0.25 (b), and 0.20 (c) (note that g_M = 0.30 was already shown in Fig. 2). Parameters: N = 500 pyramidal cells, $P(e \rightarrow e)$ = 0.10, g_{AMPA} = 0.003, $g_{K\text{-}AHP}$ = 0.8, g_{Ca} = 10, and I_{app} = 0.27. Conductances in mS/cm^2, currents in μA/cm^2.

However, each individual neuron showed the characteristic waxing and waning subthreshold oscillations (Fig. 2c2), and spikes at peaks (Fig. 2c1, arrow). Both of these features were already present in the isolated pyramidal cell shown in Figure 1.

The simulated CCH-θ was characterized by asynchronous low-frequency firing and incoherent subthreshold membrane potential oscillations. This incoherent state was unstable against increases in synaptic coupling. Increases in either the unitary excitatory synaptic conductance, $g_{AMPA}(e \rightarrow e)$, or the probability $P(e \rightarrow e)$ for synapses between cells led to population bursts. The effect of carbachol was simulated by increasing the excitability of cells and reducing the sizes of the EPSPs, as observed in experiments (there were no experimental data available on how CCH affects the connection probability or the pattern of connectivity). The reduction in EPSP size did not limit the stability of the incoherent state once it was established. However, the increased excitability did affect stability, as discussed below.

The simulations were highly sensitive to the initial state of the network. When each neuron started in an identical state, the network remained in a synchronized state. However, stochastic inputs, such as Poisson trains of EPSPs, or white noise currents could for certain parameter regimes slowly erode synchronization (not shown). This synchronized initial state is not representative of the experimental condition. The model neuron had fast variables, such as the voltage; fast voltage-dependent kinetic variables, which relaxed within about 10 ms to their steady-state values; and slow variables, such as the gating variable q of the calcium-dependent afterhyperpolarization, that relaxed on a time scale of seconds. A

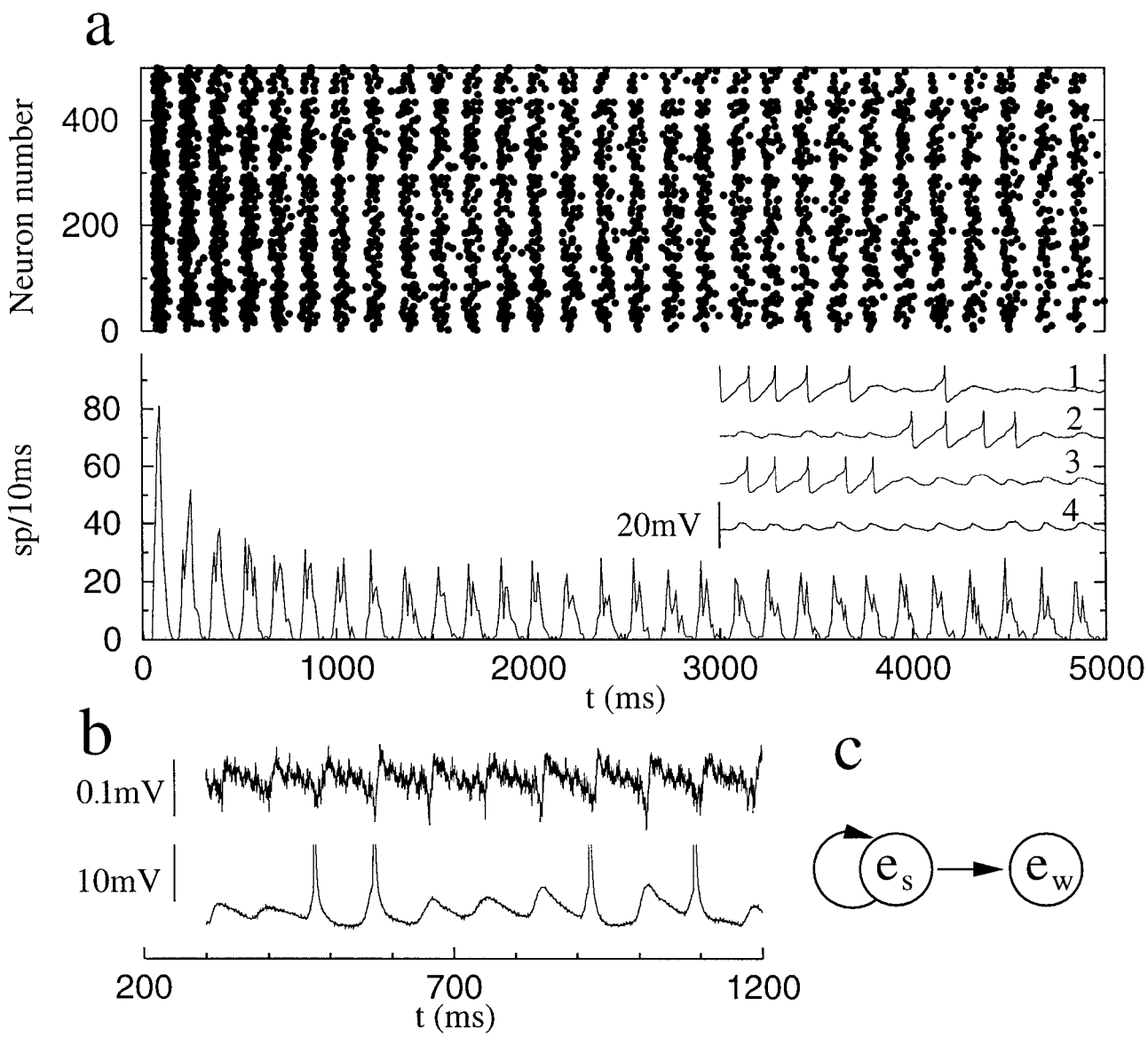

FIGURE 4. High concentrations of carbachol (13–40 μM) induced synchronous CCH-θ. a: Rastergram (top) and the firing rate histogram (bottom) for a network consisting of 50 strongly and 450 weakly connected pyramidal cells. Inset shows voltage traces from four weakly connected neurons, the time scale is unchanged, and the voltage scale is indicated. b: Experimental recording of the unfiltered field potential (top), and the intracellular voltage trace (bottom) during CCH-θ (20 μM). c: Network architecture, other parameters: $P(e_s \rightarrow e_s) = 0.5$, $g_{AMPA}(e_s \rightarrow e_s) = 0.004$, $P(e_s \rightarrow e_w) = 0.5$, $g_{AMPA}(e_s \rightarrow e_w) = 0.0012$, $I_{app,w} = 0.0$, $I_{app,s} = 0.135$, and $(g_M, g_{K\text{-}AHP}, g_{Ca}) = (0.0, 0.2, 6.0)$. Conductances in mS/cm^2, currents in μA/cm^2. Subscripts *s* and *w* indicate, respectively, the parameters of strongly and weakly connected neurons.

high q value acted as a constant hyperpolarizing current, its effect depending on the size of the $g_{K\text{-}AHP}$ conductance. The latency of the first spike as a function of initial q (or calcium concentration) had a bimodal distribution (not shown). The neuron fired either within the first 100 ms, or it fired more than 1,000 ms later (if at all). The simulations were started with random q values drawn from a uniform distribution, so that a set of neurons fired shortly after the start of the simulation (Fig. 2a), but the other neurons slowly recovered from the hyperpolarizing current. This produced minimal activity between $t = 200$ and 2,500 ms in Figure 2a.

Carbachol-Induced Synchronized Population Activity in the Delta-Frequency Range

Field potential measurements in hippocampal slices show synchronized population bursts for CCH concentrations in the range of 4–13 μM (Fellous and Sejnowski, 2000). The simulations were based on the conditions that led to these synchronized population events. First, $g_{K\text{-}AHP}$ was already reduced in the CCH concentration range during asynchronous CCH-θ; it was decreased further during CCH-δ. The greatest change oc-

curred in the reduction of muscarinic potassium conductance (Madison et al., 1987). In the following simulations only g_M was varied, showing that the effects of carbachol on g_M were in themselves enough to explain the transition to CCH-δ (Fig. 3). In addition, the average size of EPSPs decreased (Hasselmo, 1995). The possible changes due to the reduction in EPSP size on this transition are discussed later.

For $g_M = 0.35$ mS/cm^2 (13% reduction, Fig. 3a), the same asynchronous CCH-θ occurred as in Figure 2. When g_M was lowered to 0.25 mS/cm^2 (37% reduction), the average firing rate increased (after the transient). There also was a weak modulation in the network firing rate on a δ-time-scale. This was visible in the rastergram as a sequence of dark patches, alternated by light patches (Fig. 3b). The modulation in Figure 3b was not sharp enough to generate the sudden peaks in the field potential that were measured experimentally. However, lowering g_M to 0.20 mS/cm^2 (50% reduction) led to sudden population bursts of the whole network, separated by periods of lower activity of about 1000 ms in duration (Fig. 3c).

Individual neurons fired multiple spikes, or sometimes burst during the population burst, as observed experimentally (unpublished observations). The calcium that entered the neuron during the population burst increased the value of the gating variable q of the slow calcium-dependent afterhyperpolarization, $I_{K\text{-}AHP}$ (see Appendix). For sufficiently high q, the neuron stopped spiking until the resulting slow AHP had decayed. The network burst was terminated when enough neurons were in this refractive state. For a CCH-δ state to be stable, the network had to have a robust termination mechanism. Without such a mechanism the network would settle into an asynchronous state of high activity. The average network firing rate would then be flat (not shown), and would not display the characteristic CCH-δ field potentials observed experimentally. In the model, the termination depended critically on the value of $g_{K\text{-}AHP}$, which was regulated by carbachol.

Population bursts were initiated when there were enough coincident action potentials. These spikes generate enough excitation via the recurrent excitatory synapses to recruit more pyramidal cells to start an "explosive" runaway process. The minimum number n_{crit} of almost coincident spikes that was required depended on the unitary synaptic conductance and connection probability. Increasing either of these two parameters lowered n_{crit}. However, given these network parameters, whether or not n_{crit} was reached depended on the average firing rate. This was regulated by the effects of carbachol on the muscarinic potassium current (and to a lesser extent via $g_{K\text{-}AHP}$).

Although the synaptic coupling in the model remained fixed in the transition from asynchronous CCH-θ to CCH-δ, the same transition could be obtained while reducing the synaptic coupling with increasing CCH concentration. The only difference was that n_{crit} increased, and thus the necessary firing rate was higher, and consequently the necessary decrease in the value of g_M was larger (not shown).

Synchronous Oscillations in the Theta-Frequency Range

The field potentials in slice preparations oscillated at theta frequencies when the carbachol concentration was increased above 13 μM (for a review of previous experimental work, see Fellous and Sejnowski, 2000). The peak amplitude and width of the population bursts were reduced compared to the CCH-δ oscillations (Fellous et al., 1998). Intracellular recordings showed prominent membrane potential oscillations in the theta-frequency range, with spikes riding on some of the depolarizing peaks. However, during some recordings, spikes occurred in each theta cycle (not shown). CCH-θ was abolished when the fast AMPA-recurrent excitation was blocked (Williams and Kauer, 1997). This suggests that the generation of CCH-θ depends not only on intrinsic properties of the neuron, but also on network properties. This was confirmed by the results of simulations.

The physiological effects of 20 μM carbachol are diverse. The amplitudes of the muscarinic and calcium-dependent afterhyperpolarization current were almost zero (Madison et al., 1987). In addition, the calcium current was reduced (Gahwiler and Brown, 1987). Carbachol not only reduces the average size of the EPSPs, but might also change their distribution (Hasselmo, 1995). Thus there may be both weaker and stronger synapses. Simulation results indicated that the following indirect physiological consequences of carbachol could account for the transition from CCH-δ to CCH-θ (Fig. 4): a higher spontaneous firing rate and a weaker slow afterhyperpolarization. In addition, a heterogenous distribution of synaptic coupling strengths was used (see also Discussion). In particular, (g_M, $g_{K\text{-}AHP}$, g_{Ca}) was reduced to (0.0, 0.2, 6.0) mS/cm^2 (Table 1, 13–40 μM CCH), there were 50 strongly connected and 450 weakly connected pyramidal cells (Fig. 4c), and the applied currents were made more heterogeneous.

In Figure 4, the rastergram displayed synchronized oscillations in the theta-frequency range. The neurons went from a zero firing rate immediately to regular spiking at theta frequencies. Because of the recurrent excitatory connections, the strongly connected neurons fired each theta cycle. As a result, they provided a strong coherent theta-frequency drive to the weakly connected neurons. The drive resonated with the intrinsic oscillator present in each neuron, and caused a pronounced and coherent theta-frequency membrane oscillation (inset, Fig. 4a). In contrast, without the coherent synaptic drive the neurons displayed uncorrelated theta-frequency membrane oscillations. Compare the asynchronous CCH-θ in Figure 2 to voltage traces 1–3 in Figure 4a and an experimental recording in Figure 4b, in which a sequence of spikes was produced in consecutive theta-cycles.

The synchronous CCH-θ was unstable to increases in the recurrent synaptic excitation and driving current, which produced an asynchronous high firing rate state (not shown). Inhibitory neurons might under certain conditions be necessary to prevent this from occurring (see below). Of course, there is also a minimum amount of recurrent synaptic excitation necessary to sustain synchronous CCH-θ.

RESULTS: NETWORK OF PYRAMIDAL CELLS AND INTERNEURONS

Interspersed Delta- and Gamma-Frequency-Range Oscillations

During some experiments, a gamma-frequency component was found in the field potential during CCH-δ (Fellous and Sejnowski, 2000). This component had a much smaller amplitude than CCH-δ itself. The presence of gamma rhythms is usually closely associated with fast GABAergic inhibition (Whittington et al., 1995; Fisahn et al., 1998). However, applying a specific $GABA_A$ blocker did not abolish or significantly change CCH-δ. This, together with the fact that CCH-δ and CCH-γ could occur separately, suggested that they were generated by functionally distinct mechanisms. Here we studied the generation of CCH-δ and CCH-γ by adding 100 GABAergic interneurons to the model network. The pyramidal cells were divided into two groups, 250 strongly connected (e_s) and 250 weakly connected (e_w) neurons; only e_w received fast inhibitory projections from the interneurons. The resulting network architecture is shown in Figure 5e.

An important question is whether the strongly connected neurons predominantly drive the weakly connected ones, or vice versa. Figure 5 is an example of the latter case. After the initial weak burst and the transient, a series of delta-frequency-range population bursts was visible in the rastergram (Fig. 5a). The gamma-frequency component was clearly visible in the firing rate histogram. During a delta population burst, the pyramidal cells fired multiple spikes (Fig. 5d), and sometimes produced bursts (arrow in Fig. 5b). Theta-frequency subthreshold oscillations reappeared in the voltage trace after the population-burst-induced slow AHP had decayed (indicated by asterisks in Fig. 5b).

The weakly coupled neurons received a GABAergic projection. We assumed that the interneurons were tonically active due to the carbachol-induced depolarization and enhanced excitability (Freund and Buzsaki, 1996; Fellous and Sejnowski, 2000). There might also be a contribution from excitatory synaptic projections, although that was not included in our present example (but see below). A model network consisting of heterogeneous and noisy interneurons coupled by mutual inhibition can generate a gamma-frequency population rhythm (Traub et al., 1996a; Tiesinga and José, 2000a). Our interneuron network indeed synchronized after a transient. The length of the transient depended on the variance in the distribution of voltage values at the start of the simulation. In the example shown in Figure 5, they were synchronized within the first 10 ms of the simulation. This was visible as a regular series of IPSPs in the membrane potential of the pyramidal cell (Fig. 5c). The pyramidal cell only fired once every few gamma cycles, yielding a low average firing rate. The waxing and waning of CCH-γ was an effect of the random initial condition (see arrows in Fig. 5a and horizontal line in Fig. 5c). The waxing and waning were more pronounced when weak recurrent excitation between neurons was included, and the constant injected current drive could then be reduced. The functional role of waxing and waning for the stability or induction of CCH-γ is unclear at present.

Because of the coupling from e_w to e_s, gamma-band activity occurred shortly before the onset of a delta burst. However, the increased CCH-γ did not always lead to a population burst (see arrows in Fig. 5a). Population bursts only occurred when the slow AHP induced by the previous population burst had sufficiently decayed. In that way, the delta bursts still occurred approximately once a second.

Interspersed Theta- and Gamma-Frequency Oscillations

Interspersed oscillations in the gamma and theta frequency range have been observed in field potential recordings from the hippocampal slice (Fellous and Sejnowski, 2000). The dynamics of the CCH-θ network were examined in the presence of tonically active inhibitory interneurons (Fig. 6d), without changing the intrinsic properties of the pyramidal cell model. Inhibitory synapses were added to 100 of the weakly connected neurons, and the applied constant current to them was increased. Figure 6 shows an example of the oscillations obtained in this model. The rastergram (Fig. 6a) looked noisier compared to the one in Figure 4. This is because the theta and gamma component had a similar amplitude, and although firing was reduced in the trough of the theta cycle, it was not terminated completely. The activity of neurons without GABAergic innervation (Fig. 6b) looked similar to the activity shown in Figure 4. The gamma component (Fig. 6c) was similar to that described above, since its generation by GABAergic interneurons was to a large extent uncorrelated with the underlying pyramidal cell activity.

Isolated Gamma-Frequency Oscillations

Gamma-frequency oscillations have also been observed experimentally in isolation from other rhythms (Fisahn et al., 1998; Fellous and Sejnowski, 2000). In Figures 5 and 6, the tonically active interneuron network provided the necessary synaptic drive to obtain pyramidal-cell gamma rhythms. The dynamics of the interneuron-pyramidal cell network responsible for the gamma rhythms were examined, and two ways were found to make a population of pyramidal cells spike at gamma frequencies, called γ-I and γ-II. In γ-I (Fig. 7a,b,d), the interneurons provided a constant inhibitory drive to which the pyramidal cells were entrained. Some pyramidal neurons fired spontaneously at a low rate in the presence of inhibition; others needed some stochastic noise to fire during the troughs of the inhibitory drive. A pyramidal cell only fired when the inhibition was coherent, at least for the parameter values considered in Figure 7d. From random initial conditions, it took 1,000 ms for the interneurons to synchronize in Figure 7d. During the long transient period, the pyramidal cells did not fire because the asynchronous interneuron network provided a tonic, rather than phasic, inhibition that hyperpolarized the pyramidal cells.

In Figure 7a, gamma activity was inhomogeneous: during some cycles many neurons fired, whereas on other cycles almost none fired. This was a consequence of the initial conditions. Stochastic noise or a weak recurrent excitation could smooth out the inhomogeneity. In Figure 7b a noise current was injected into the

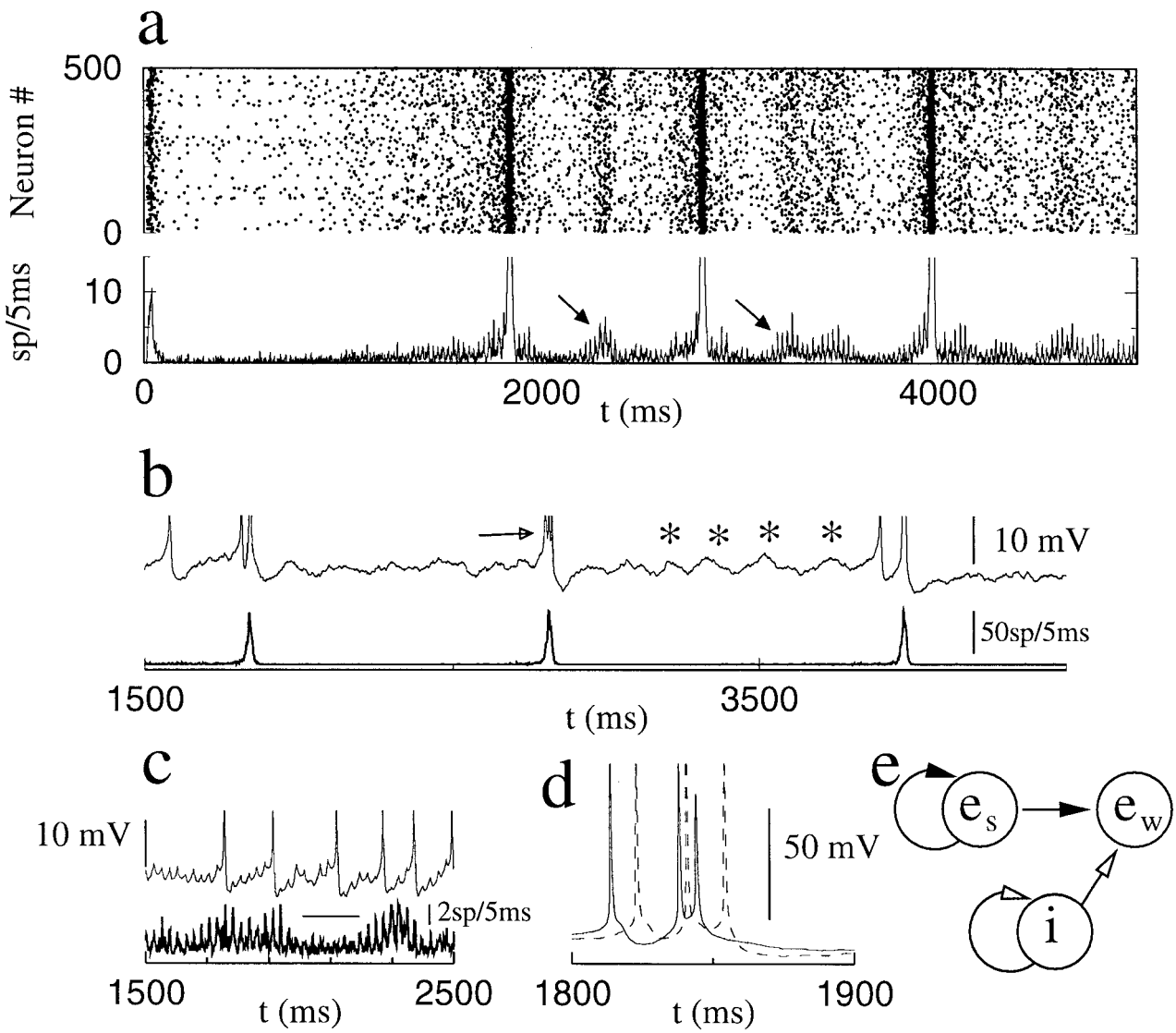

FIGURE 5. Interneuron-pyramidal cell interactions generated interspersed CCH-δ and CCH-γ activity. The simulated network consists of 250 strongly, and 250 weakly connected pyramidal cells, and 100 inhibitory interneurons projecting to the weakly coupled neurons. a: Rastergram (top) and firing rate histogram (bottom). Activity during the delta burst has been truncated. Arrows indicate spontaneous gamma-frequency-range oscillations. b: Firing rate histogram (bottom) of strongly connected cells, and an example voltage trace (top) of one of these cells. Asterisks indicate subthreshold membrane oscillations in the theta-frequency range. Arrow indicates a burst in intracellular voltage. c: Firing rate histogram (bottom) of weakly connected neurons, and membrane potential (top) of one of these neurons. d: Closeup of voltage traces of two strongly connected neurons. We show firing rate scale bars for 50 and 2 spikes/5 ms in b and c, respectively, and voltage scale bars for 10 mV in b and c, and 50 mV in d. e: Network architecture, other parameters: $P(e_s \rightarrow e_s) = 0.2$, $g_{AMPA}(e_s \rightarrow e_s) = 0.005$, $P(e_w \rightarrow e_s) = 0.1$, $g_{AMPA}(e_w \rightarrow e_s) = 0.0011$, $P(i \rightarrow e_w) = 1.0$, $g_{GABA}(i \rightarrow e_w) = 0.002$, $P(i \rightarrow i) = 1.0$, $g_{GABA}(i \rightarrow i) = 0.001$, $I_{app,w} = 1.35 \pm 0.05$, $I_{app,s} = 0.27$, $I_{int} = 1.0$, and (g_M, $g_{K\text{-}AHP}$, g_{Ca}) = (0.2, 0.8, 10.0). Conductances in mS/cm^2, currents in μA/cm^2. Subscripts *s* and *w* indicate, respectively, the parameters of strongly and weakly connected neurons.

pyramidal cells. Gamma activity was only stable for weak recurrent excitation. Slightly stronger interactions (e.g., $g_{AMPA} > 0.001$ mS/cm^2) could lead to large amplitude fluctuations of the gamma oscillation, theta-frequency activity, or population bursts (not shown).

γ-II occurred when there was excitatory feedback from the pyramidal cells to the interneurons, providing the interneurons with a phasic synaptic drive in addition to a tonic current drive (Fig. 7c). First, pyramidal cells fired, producing the excitation that recruited the interneurons. Second, the inhibition generated by the spiking interneurons stopped the pyramidal cell activity for one gamma cycle. The length of the cycle was determined by the precision of the interneuron discharge, and the time constant of the GABAergic synapse onto the pyramidal cell. This was different from γ-I, where the time-scale was set by the kinetics of the recurrent synapses of inhibitory interneurons onto themselves. The temporal jitter in the interneuron firing times determined the size of the phasic vs. tonic inhibition. Tonic inhibition hyperpolarized neurons, and phasic inhibition patterned the discharge. A temporal dispersion in the pyramidal cell discharge led to a less precise in-

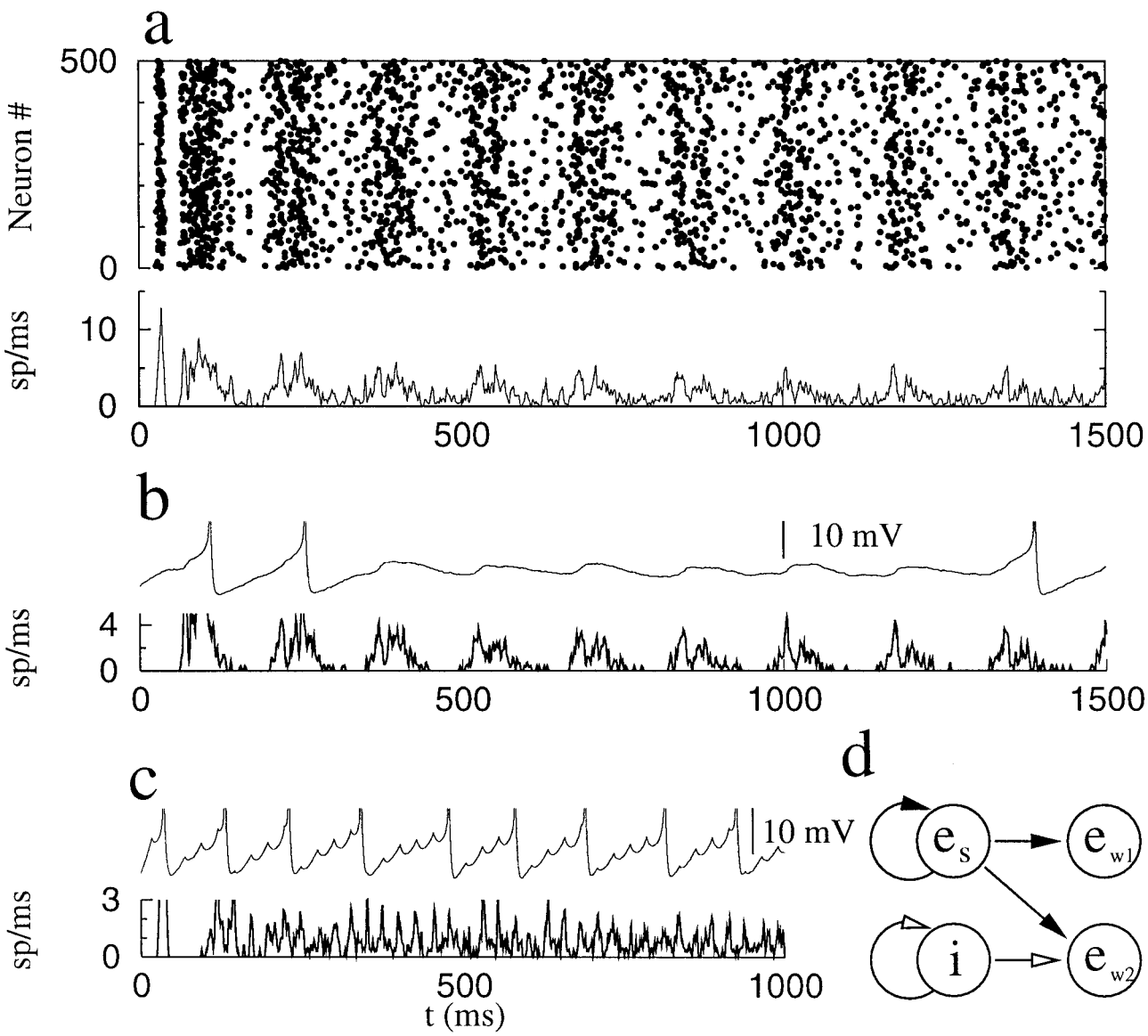

FIGURE 6. Activation of interneuron network during CCH-θ produced interspersed CCH-θ and CCH-γ oscillations. The network had 500 pyramidal cells and 100 interneurons. Fifty pyramidal cells were strongly connected, 450 were weakly connected, and 100 of the latter received inhibitory projections. a: Pyramidal cell rastergram (top) and firing rate histogram (bottom) (bin width, 1 ms). b, c: Firing rate histogram (bottom) and voltage traces (top) of one of the neurons, for (b) the pyramidal cells that did not receive an inhibitory projection, and (c) those that did receive an inhibitory projection. Network architecture is shown in d. Other parameters: $P(e_s \rightarrow e_s) = 0.5$, $g_{AMPA}(e_s \rightarrow e_s) = 0.004$, $P(e_s \rightarrow e_{w1}) = 0.5$, $g_{AMPA}(e_s \rightarrow e_{w1}) = 0.0012$, $P(e_s \rightarrow e_{w2}) = 0.5$, $g_{AMPA}(e_s \rightarrow e_{w2}) = 0.0002$, $P(i \rightarrow e_{w2}) = 1.0$, $g_{GABA}(i \rightarrow e_{w2}) = 0.002$, $P(i \rightarrow i) = 1.0$, $g_{GABA}(i \rightarrow i) = 0.001$, $I_{app,w1} = 0.0 \pm 0.05$, $I_{app,w2} = 1.05 \pm 0.05$, $I_{app,s} = 0.135$, $I_{int} = 1.0$, and $(g_M, g_{K\text{-}AHP}, g_{Ca}) = (0.0, 0.0, 6.0)$. Conductances in mS/cm^2, currents in μA/cm^2. Subscripts *s* and *w1*, *w2* indicate, respectively, the parameters of strongly connected neurons, and of weakly connected neurons without and with GABAergic innervation.

terneuron discharge, which in turn led to a reduced pyramidal cell firing rate. The complex oscillation that resulted depended sensitively on the relative strengths of the $i \rightarrow e$ and $e \rightarrow i$ connection. For sufficiently strong excitation, multiple interneuron spikes per cycle were generated. This stopped the pyramidal cell discharge for a longer time, and increased the number of nonrefractory pyramidal neurons. This destabilized the gamma oscillations and could in some circumstances lead to population bursts (not shown).

Field Potential Oscillations With Gamma, Theta, and Delta Frequency Components

During some simulations, the model network showed highly complex dynamical behavior. An example of network dynamics at medium CCH concentrations with all three frequencies present is shown in Figure 8. This oscillation has not yet been observed in slice preparations. The network in Figure 8c consisted of 100 interneurons and 500 pyramidal cells (250 weakly and 250 strongly

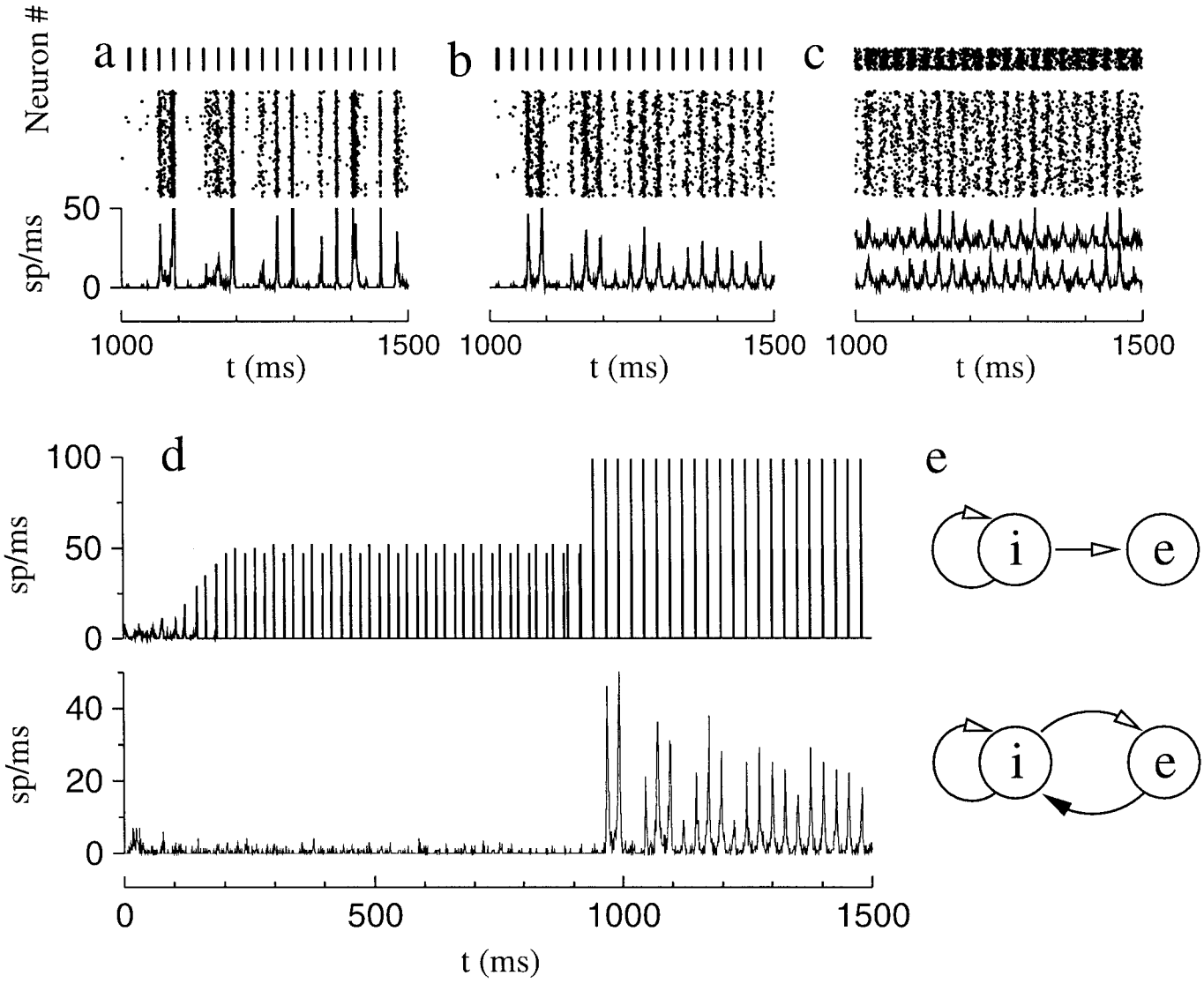

FIGURE 7. Two distinct mechanisms, γ-I and γ-II, could produce gamma rhythms in a network with inhibitory interneurons. The network had 500 pyramidal cells and 100 interneurons. a–c show, from top to bottom, the interneuron rastergram, the pyramidal cell rastergram and the pyramidal cell firing rate histogram (bin width, 1 ms). a, b: γ-I, pyramidal cells only receive an inhibitory synaptic drive and are driven by (a) a constant current and (b) a current with white noise. c: γ-II, pyramidal cells project back to the interneurons. d: Firing rate histogram in b replotted over the full length of the simulation, for interneurons (top) and pyramidal cells (bottom). e: Network architecture for γ-I (top) and γ-II (bottom), parameters: $P(i \rightarrow e) = 0.2$, $g_{GABA}(i \rightarrow e) = 0.02$, $P(i \rightarrow i) = 1.0$, $g_{GABA}(i \rightarrow i) = 0.001$, $I_{int} = 1.0$, $(g_M, g_{K\text{-}AHP}, g_{Ca}) = (0.0, 0.4, 6.0)$. Specific parameters: (a) $I_{app} = 1.35$, (b, d) $I_{app} = 1.35$, white-noise variance $D = 0.02$ mV^2/ms, (c) $I_{app} = 2.70$, $P(e \rightarrow i) = 0.1$, $g_{AMPA}(e \rightarrow i) = 0.01$. Conductances in mS/cm^2, currents in μA/cm^2.

connected, labeled by *w* and *s*, respectively). The sequence of events, labeled in Figure 8, was:

I. A burst was generated by the initial conditions.
II. The weak population recovered from the refractive period and oscillated in the gamma-frequency range under the influence of the synchronized interneurons.
III. The weak population activated the strong population that had sufficiently recovered from the refractive period. A delta burst was generated.
IV. The delta burst generated multiple interneuron spikes. The inhibition stopped all activity. The delta burst also desynchronized the interneuron network.
V. When the interneuron network resynchronized, a large part of the weak population was ready to fire. The recurrent excitation drove the network to interspersed gamma and theta activity.

The scenario III–V then repeated itself.

DISCUSSION

Physiologically plausible mechanisms for CCH-δ, CCH-θ, and CCH-γ rhythms (Fellous and Sejnowski, 2000) are suggested by

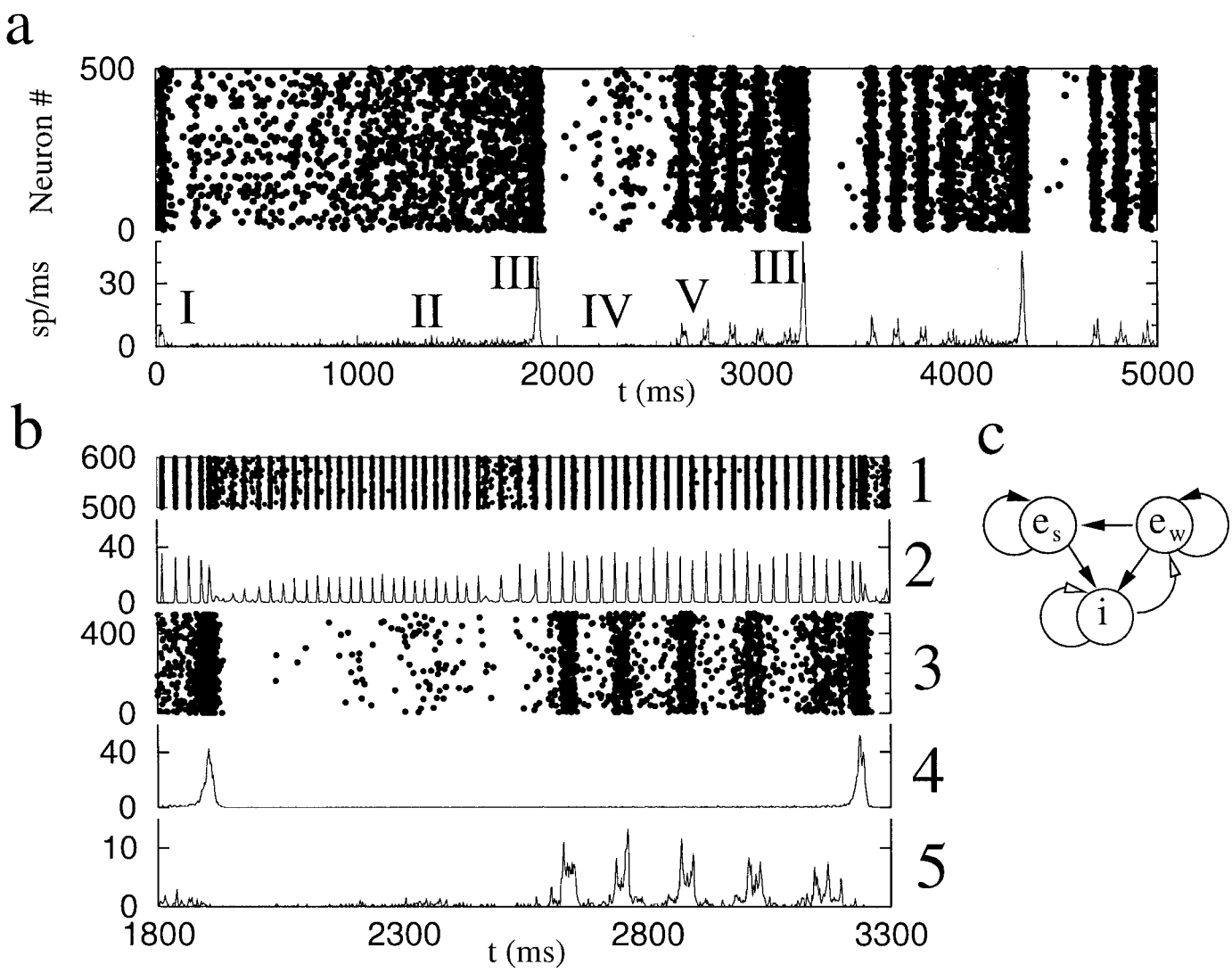

FIGURE 8. Coupling between CCH-γ, CCH-δ, and subthreshold membrane potential oscillations generated complex field potential dynamics. a: Pyramidal cell rastergram (top) and firing rate histogram (bottom) (bin width, 1 ms). Different stages of the oscillation are indicated with Roman numerals (see text). b: Higher resolution rastergrams of (1) interneurons and (3) pyramidal cells, and firing rate histograms of (2) interneurons and (4) strongly connected and (5) weakly coupled pyramidal cells. c: Network architecture, parameters: $P(e_s \rightarrow e_s) = 0.2$, $g_{AMPA}(e_s \rightarrow e_s) = 0.005$, $P(e_w \rightarrow e_s) = 0.1$, $g_{AMPA}(e_w \rightarrow e_s) = 0.0022$, $P(e_w \rightarrow e_w) = 0.04$, $g_{AMPA}(e_w \rightarrow e_w) = 0.011$, $P(e_{w/s} \rightarrow i) = 0.2$, $g_{AMPA}(e_{w/s} \rightarrow i) = 0.001$, $P(i \rightarrow e_w) = 1.0$, $g_{GABA}(i \rightarrow e_w) = 0.002$, $P(i \rightarrow i) = 1.0$, $g_{GABA}(i \rightarrow i) = 0.001$, $I_{app,w} = 1.35 \pm 0.05$, $I_{app,s} = 0.27$, $I_{int} = 0.9$, and $(g_M, g_{K\text{-}AHP}, g_{Ca}) = (0.2, 0.8, 10.0)$. **Conductances in mS/cm^2, currents in μA/cm^2. Subscripts *s* and *w* indicate the parameters of strongly and weakly connected neurons, respectively.**

the simulations reported here. The known cellular and synaptic effects of carbachol can explain the transitions between these different rhythms. The model also makes predictions that can be experimentally tested.

Physiological Substrates of Oscillation Time-Scales

In the network model, the time scale for CCH-δ was set by the decay rate $t_{K\text{-}AHP}$ of the gating variable q of the calcium-dependent potassium current. The amount of applied current I_{app} determined the value of q at which the spiking threshold would be reached. This led to a relative refractive period between 500–1,500 ms, corresponding to delta oscillations between 0.5–2 Hz. We performed simulations in which we varied $t_{K\text{-}AHP}$ to determine how the network oscillation frequency f during CCH-δ would be affected (Fig. 9a). The oscillation frequency decays almost linearly with $t_{K\text{-}AHP}$ up to $t_{K\text{-}AHP} = 800$ ms.

Other currents exist that have gating variables with a similarly slow dynamics. Recent investigations show that the slowly inactivating outward potassium (I_{KS}) current may underlie bursting in a putative respiratory pacemaker nucleus in the brainstem (Butera et al., 1999a,b). It is not known whether this or other currents are present in hippocampal cells to a large enough extent to contribute to the network behavior during CCH-δ, or to what extent they are

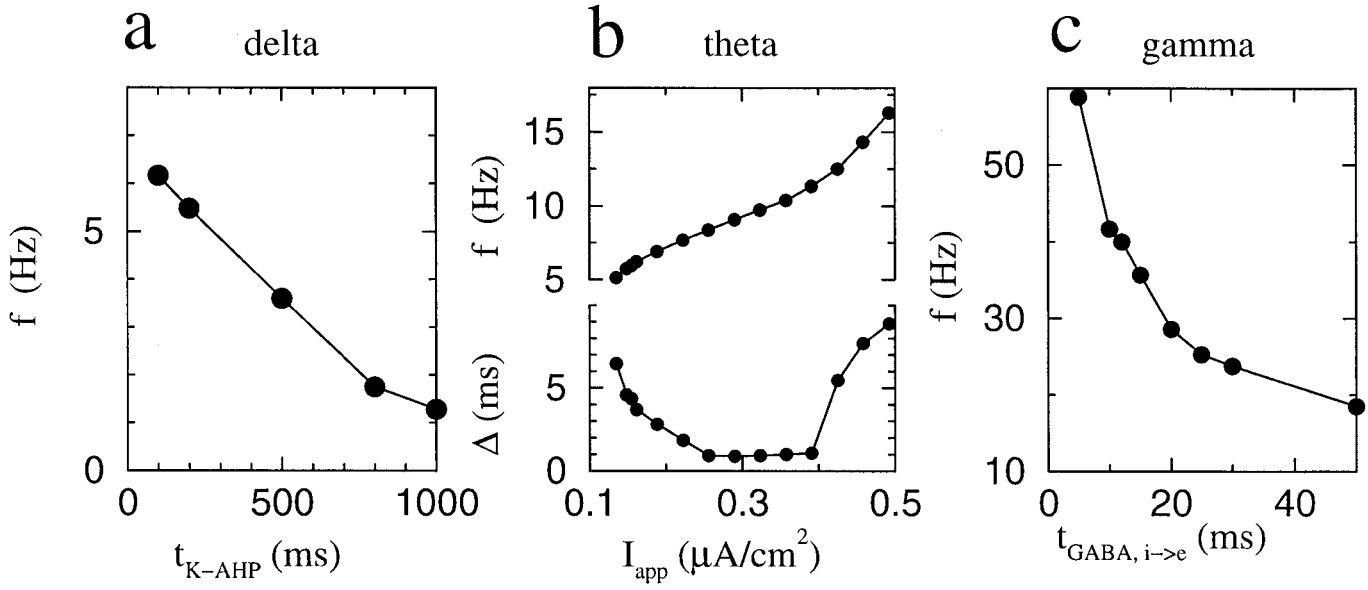

FIGURE 9. Oscillation frequencies of CCH-δ, -θ, and -γ depend on specific biophysical parameters. a: Burst frequency during CCH-δ as a function of the decay constant $t_{K\text{-}AHP}$ of the gating variable q of $I_{K\text{-}AHP}$ (see Appendix). Network parameters are as in Figure 3c. b: Frequency (top) and temporal dispersion Δ (bottom) of CCH-θ as a function of the driving current I_{app} to the pyramidal cells. Network parameters are the same as for the strongly coupled network (e_s) in Figure 4. c: Frequency of CCH-γ as a function of the decay constant $t_{GABA,i\to e}$ of the fast GABAergic synapses. Parameters as in Figure 7c.

modulated by carbachol. The distinguishing feature between I_{K-AHP} and I_{KS} is the dependence on calcium entry into the cell, which would be amenable to experimental verification, e.g., using calcium imaging (Denk et al., 1994; Peterlin et al., 2000).

The time scale for CCH-θ was determined by a subthreshold intrinsic membrane potential oscillation. Persistent-like sodium (I_{NaO}) and potassium (I_{KO}) currents were added to the model, and their kinetics were tuned using phase-plane analysis (White et al., 1995), such that the currents were active slightly above the resting membrane potential and resonated between 5–10 Hz, in agreement with experimental results presented here and elsewhere (Leung and Yim, 1991). The frequency of membrane potential oscillations is set by our choice of parameters for I_{KO} and I_{NaO}. Any change in these parameters could also change the frequency (not shown). However, the firing rate of the neuron also depends on the amount of driving current I_{app} (or depolarization). In Figure 9b we show how the network oscillation frequency f varies with I_{app}. The network only oscillates above a certain minimum frequency, set by the subthreshold mode, approximately equal to 5 Hz for the present parameter set. We determined the standard deviation Δ of the spike times of all neurons in one cycle, averaged over all cycles. The coherence or synchronization of the oscillation depends inversely on Δ. The larger Δ is, the less effective the resulting synaptic drive is in synchronizing other neurons. We find that oscillation is only coherent in a particular current range, so that the observed frequencies are essentially restricted to the theta range. Increasing the strength of the recurrent excitatory unitary conductance reduces the width of this coherent current range. In order to test the model prediction, one could depolarize pyramidal cells through the activation of metabotropic glutamate receptors or any other means that would uniformly depolarize neurons.

Resonances and subthreshold oscillations have been found in a variety of different neurons (see below). In most cases, the underlying currents have not been identified with certainty. In the present work, the consequences of the presence of subthreshold membrane potential oscillations on the network behavior were explored through simulations.

Gamma oscillations have attracted experimental and theoretical attention (Wang and Buzsáki, 1996; White et al., 1998a; Tiesinga and José, 2000a; Traub et al., 1996b). Fast GABAergic synapses between inhibitory interneurons are the main generator of this rhythm in hippocampal slices (Whittington et al., 1995). The same mechanism may be responsible for CCH-γ, as suggested by the experimental results of Fisahn et al. (1998). It was shown in previous studies (Traub et al., 1996a; Chow et al., 1998) that the oscillation frequency during γ-I is determined by the decay constant of the mutual inhibition $t_{GABA,i\to i}$. In γ-II it is set by the time constant of the inhibitory synapse on the pyramidal cells. The network frequency f depends inversely on $t_{GABA,i\to e}$ (Fig. 9c). Although $t_{GABA,i\to i}$ does not affect the oscillation frequency directly, it still is an important physiological variable. In order for the interneuron network to synchronize to the phasic excitatory input, $t_{GABA,i\to i}$ and the interneuron driving current have to be chosen carefully. In simulations where $t_{GABA,i\to i}$ was kept fixed at 10 ms while $t_{GABA,i\to e}$ was increased, the oscillation became less and less coherent. For that reason we have set $t_{GABA,i\to i} = t_{GABA,i\to e}$ in Figure 9c. Our model predictions can be tested by modifying GABAergic time constants, using barbiturates and benzodiazepines (Whittington et al., 1995; Traub et al., 1996a).

Physiological Requirements

The presence of asynchronous CCH-θ, CCH-δ, CCH-θ, and CCH-γ, together with the known effects of carbachol on the intrinsic and synaptic properties of neurons, imposed a set of constraints on models. The key features underlying each type of oscillation are summarized below.

Asynchronous CCH-θ was obtained when there was enough depolarization to activate the subthreshold membrane oscillations, consistent with in vitro and in vivo data (Bland and Colom, 1993; Fellous and Sejnowski, 2000). Some source of stochasticity may be required to generate action potentials riding on top of the depolarization. Similar results are found with either intrinsic noise or random trains of incoming EPSPs. The incoherent state is destabilized by a high level of spontaneous activity. The maximum amount of spontaneous activity is therefore an important physiological variable. Its value for a given network depends on the size of the unitary excitatory conductance, and the probability of making a synaptic connection.

CCH-δ was obtained when the low spontaneous firing rate state was "unstable" and the unitary conductance and connectivity were large enough to create a runaway process of recruitment of pyramidal cells via recurrent excitation. The resulting high-activity-state population burst can be terminated by an intrinsic mechanism, or a short-term synaptic modification process (Koch, 1999). In the simulations, $g_{K\text{-}AHP}$ was large enough compared to the recurrent excitation to terminate the burst. The role of $I_{K\text{-}AHP}$ can be investigated experimentally by blocking it with a selective blocker such as apamin. Our model then predicts an asynchronous high-activity state.

Coherent CCH-θ occurred when a subgroup of neurons was depolarized enough to spike in the theta-frequency range. Furthermore, the adaptation currents, $g_{K\text{-}AHP}$ in combination with the calcium current g_{Ca}, and g_M, were reduced under the influence of carbachol, so that they did not terminate the spiking. In our experiments we found pyramidal cells that fired spikes each theta cycle during CCH-θ activity in the field potential, and cells that skipped cycles. We assume that during CCH-θ both types of single-cell activity were present. We did not find this mix of single-cell activity in networks with a homogeneous distribution of synaptic strength and intrinsic properties. Hence, to reproduce this network state, we assumed that the amount of depolarization of the neurons was different for the two behaviors. This difference could either arise from differences in intrinsic properties, or from differences in the amount of excitatory input the neuron received. We explored the consequences of the latter assumption in model simulations, though we do not exclude the former assumption. We approximated the heterogeneity in the synaptic coupling by a bimodal distribution, creating two subpopulations, one weakly coupled and one strongly coupled. How did this heterogeneity come about? One possibility is that a high concentration of carbachol induces heterogeneity directly or via synaptic plasticity. There indeed is evidence that CCH differentially modulates the strength of synapses in different layers of CA1 onto the same CA1 pyramidal cell (Hasselmo and Schnell, 1994). However, at present, there is no indication that carbachol would differentially affect the strength of the recurrent excitatory synapses in CA3.

Another likely possibility is that the slice is heterogeneous from the start. We have performed simulations of asynchronous CCH-θ and CCH-δ in the same heterogenous network as for the synchronous CCH-θ in Figure 4. We find the same behavior as before. Further experiments are needed to determine what mechanism underlies the heterogeneity in CA3.

There was earlier experimental work on CCH-θ in CA3 (Williams and Kauer, 1997; Fischer et al., 1999). In Williams and Kauer (1997), pyramidal cells fire bursts on each theta cycle. This is similar to the oscillations modeled in Traub et al. (1992) and the activity of the strongly coupled network in the simulations (though the model neurons fire single spikes). On the other hand, Fischer et al. (1999) reported that pyramidal cells fire synchronously but only on very few theta cycles. This behavior is similar to that of our weakly coupled network. In contrast, Fisahn et al. (1998) found only CCH-γ that is sometimes modulated at θ-frequencies. These authors suggest that differences between these experimental results are due to "slight differences in the preparation (horizontal vs. transverse slices) or external medium (for example, potassium concentration)" (Fisahn et al., 1998).

CCH-γ depended on activating networks of interneurons via carbachol-induced depolarization. The number of active interneurons was large enough and had a high enough connection probability so that they synchronized. For the γ-I mechanism to be effective, each interneuron needs to receive at least 60 synapses from other interneurons (Wang and Buzsáki, 1996). A group of pyramidal cells should also be sufficiently depolarized by carbachol to fire during the troughs of the synchronized inhibition from the interneurons.

We described two mechanisms for generating CCH-γ, γ-I and γ-II. An important question is whether both occur at the same time and interact, or whether one would be dominant during CCH-γ. Experiments (Fisahn et al., 1998) provide two important constraints on the mechanism: the gamma oscillations in the field potentials are abolished when fast inhibition, $GABA_A$, or AMPA synapses are blocked. The first constraint is satisfied by both mechanisms: by blocking $GABA_A$ synapses there is no inhibitory synaptic drive that prevents pyramidal neurons from firing out of phase. The second constraint is also satisfied by γ-II. When there is no AMPAergic excitatory drive to the interneurons, they will fire at low frequencies, or not fire at all. In either case there will not be a coherent inhibitory drive at gamma frequencies. For γ-I the case is more subtle. In the absence of recurrent excitation, the pyramidal cells may not be depolarized enough to fire in the presence of inhibition. As a result, the oscillations in the field potential would disappear. However, one should still be able to measure subthreshold synchronized IPSPs in the pyramidal-cell membrane potential (Whittington et al., 1995). For that reason we currently favor the hypothesis that γ-II dominates during CCH-γ. There are two manipulations that would yield further quantitative differences between γ-I and γ-II. The pyramidal cells should fire on more cycles during γ-I for increasing depolarization, but the oscillation frequency should not increase. During γ-II, however, the excitatory drive to the interneurons would also increase, hence changing

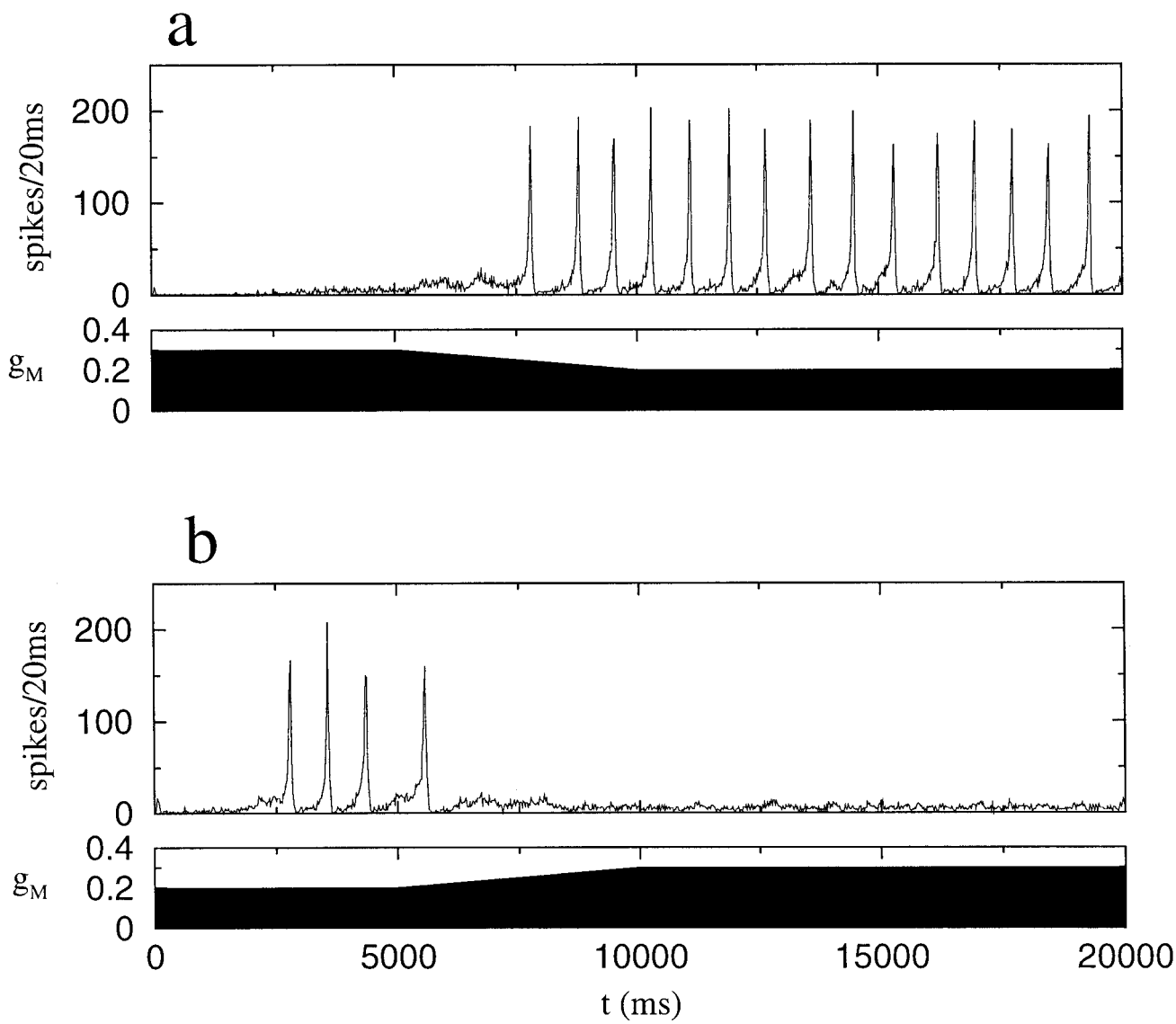

FIGURE 10. Transition between asynchronous CCH-θ and CCH-δ can be generated by reducing g_M. In a and b, firing rate histogram is at top, value of g_M vs. time is on bottom. a: g_M is decreased from 0.3 to 0.2 mS/cm^2. b: g_M is increased from 0.2 to 0.3 mS/cm^2. Other parameters are as in Figure 3.

the frequency. As mentioned before, the frequency of the γ-I scales with the time constant of mutual inhibition ($t_{GABA,i\to i}$), whereas that of γ-II varies with the time constant ($t_{GABA,i\to e}$) of inhibition onto pyramidal cells. Therefore, one could distinguish between γ-I and γ-II, if one could independently modify the characteristics of the inhibitory synapses on interneurons and pyramidal cells.

Transition Between Different Frequency Ranges Under the Control of Carbachol

Cholinergic modulation can affect the type of oscillation that is stable. We show here how the known physiological effects of carbachol can switch the network oscillations from asynchronous CCH-θ to CCH-δ, and from CCH-δ to CCH-θ.

Low concentrations of carbachol (1–4 μM CCH) depolarize pyramidal cells (Madison et al., 1987; Fellous and Sejnowski, 2000), activate the subthreshold membrane oscillations, and sometimes induce spikes riding on the depolarized part of the oscillations. Higher carbachol concentrations (4–13 μM CCH) increase the spontaneous firing rate in vitro (via reduction of g_M and g_{K-AHP}, and additional depolarization), destabilize the low firing rate state, and induce CCH-δ bursts. Carbachol increases the spontaneous firing rate, but reduces the average unitary excitatory conductance. The increase in firing rate therefore dominates the effect of reduced EPSP size. The transition between incoherent CCH-θ and CCH-δ can be induced by gradually reducing g_M (Fig. 10a). This transition is reversible: gradually increasing g_M turns CCH-δ back into asynchronous CCH-θ.

At higher carbachol concentrations (13–40 μM CCH), the last remnants of adaption currents are blocked and synchronized bursts in CCH-δ become unstable. Simulations of these conditions typ-

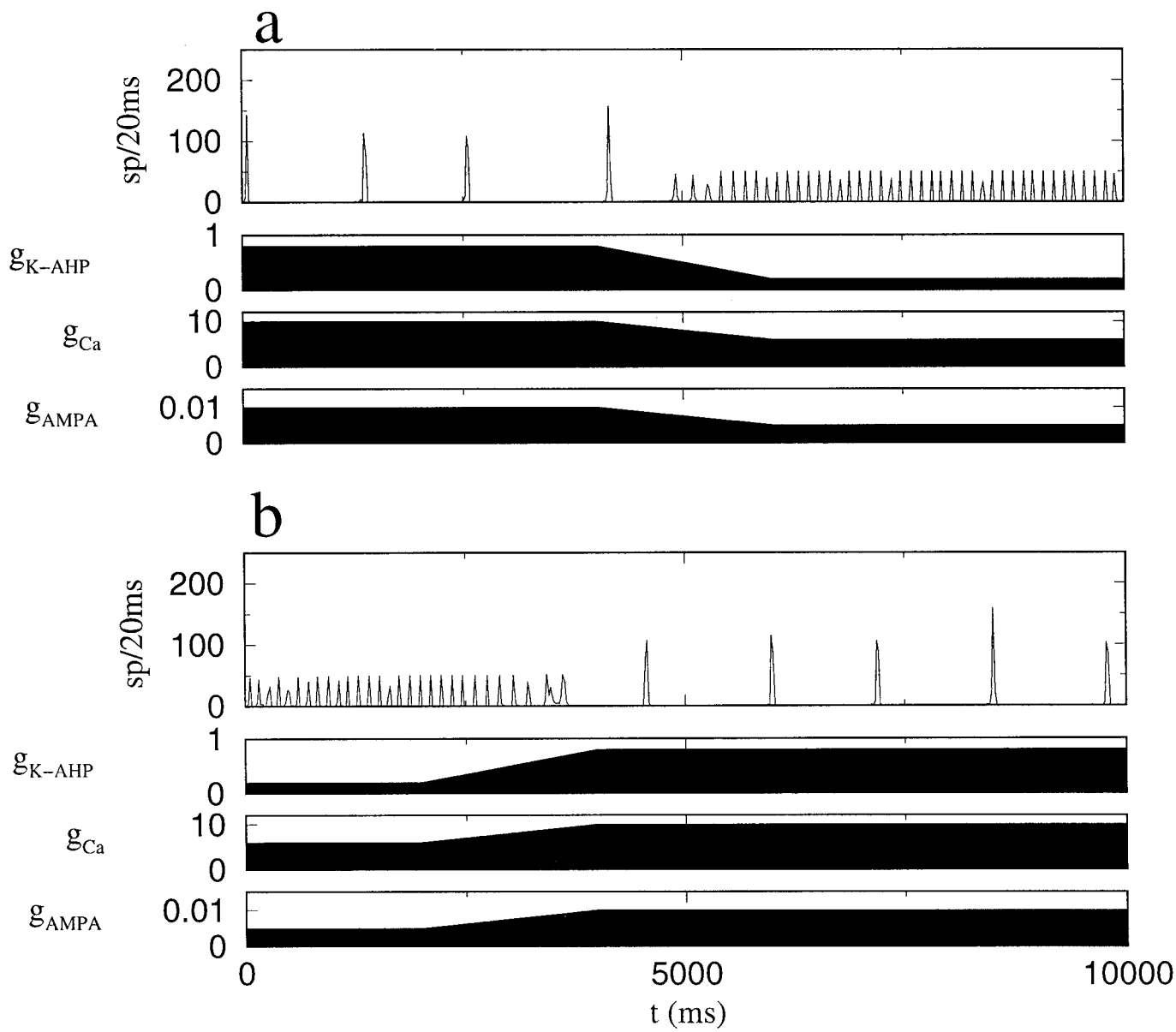

FIGURE 11. Transition between CCH-δ and CCH-θ can be induced by reducing $g_{K\text{-}AHP}$, g_{Ca}, and g_{AMPA}. In a and b, top to bottom: firing rate histogram, $g_{K\text{-}AHP}$, g_{Ca}, and g_{AMPA} vs. time. a: Parameters are gradually changed from their values for medium carbachol concentration to those at high carbachol concentration (Table 1, except that $g_M = 0$). b: Change from high to medium carbachol concentration. Other parameters are as for the strongly connected network (e_s) in Figure 4.

ically display either CCH-θ or an asynchronous state with high firing rates. In Figure 11a, we induce the transition from CCH-δ to CCH-θ by gradually changing the parameter values of the pyramidal cells from those at medium to those at high carbachol concentration (Table 1) and gradually reducing the synaptic strength by 50%. The transition is reversible, as shown in Fig. 11b.

In the model, the presence of CCH-γ is independent from CCH-δ and CCH-θ, consistent with experiments (Fisahn et al., 1998; Fellous and Sejnowski, 2000). However, it only occurs when the carbachol concentration is high enough to activate many interneurons and pyramidal cells. The population of pyramidal cells that participate in CCH-γ may overlap to a certain extent with those that participate in CCH-δ and CCH-θ. This is also consistent with experimental results that show that the amplitude and frequency of theta and gamma oscillations are correlated (Bragin et al., 1995).

Comparison to Previous Work, and Future Work

The explanations proposed here for the different carbachol-induced rhythms are testable. The results of the model also suggest new avenues for experiments and theory. Here we discuss previous work and possible extensions.

Effect of carbachol-induced changes

The effects of acetylcholine on the intrinsic properties of pyramidal cells and interneurons are wide-ranging and only partly un-

derstood. Carbachol, a muscarinic agonist, reduces $I_{K\text{-}AHP}$ (Cole and Nicoll, 1983, 1984a,b), I_A (Nakajima et al., 1986), I_M (Brown and Adams, 1980; Halliwell and Adams, 1982), calcium currents (Gahwiler and Brown, 1987), and a resting potassium current (Madison et al., 1987; Benson et al., 1988). Dose-response curves for these effects have been published or can be derived from published experimental results. Menschik and Finkel (1998, 1999) implemented the dose-response curves for carbachol in detailed biophysical models. They found that increasing CCH concentration turns an intrinsically bursting CA3 pyramidal cell into a regular spiking one. However, the precise mechanism for the CCH-induced transition from bursting to spiking is still unknown. Migliore et al. (1995) suggest that increasing I_A leads to regular spiking, whereas Menschik and Finkel (1998, 1999) show instead that decreasing I_A is sufficient to go from bursting to doublet spiking. Furthermore, increasing the membrane potential or increasing driving current alone can also induce this transition (Pinsky and Rinzel, 1994; Traub et al., 1991). This is consistent with the fact that CCH causes a depolarization. In addition, changes in the relative electronic length of the soma and dendrite can also induce a similar transition (Mainen and Sejnowski, 1994). Clearly the detailed cellular effects of carbachol on neuronal dynamics require further theoretical and experimental study.

How do these currents switch the network from one frequency range to another? To explore this issue, the carbachol spectrum was divided into three regimes, and only one or two currents were varied during each simulation run. The other currents were fixed in a physiologically realistic range, consistent with experimental data (see Methods). This led to hypotheses about the functional relevance of the $I_{K\text{-}AHP}$ and I_M current in generating transitions.

We also constructed a subthreshold oscillation mode and added it to our model neuron. Unlike previous models for subthreshold oscillations (White et al., 1998b), it included internal calcium dynamics and a slow calcium-dependent AHP. However, we did not address the issue of the currents responsible for this subthreshold mode in the pyramidal cells or how these currents are modulated by carbachol. This is an important question that should be studied with compartmental models of reconstructed cells, since morphology might be a relevant factor.

Network oscillation mechanisms

Synchronized oscillations should be robust against the imperfections present in real neural circuitry including initial conditions, neuronal heterogeneity, presence of intrinsic and synaptic noise, and sparse and stochastic connectivity. In the model, these issues were examined for each of the oscillations, but not for all the frequency ranges at the same time or the transitions between them.

The robustness of synchronization by mutual inhibition, γ-I, has been studied in some detail (Wang and Buzsáki, 1996; Traub et al., 1996a; White et al., 1998a; Tiesinga and José, 2000a). In principle, two types of synchronization can result: strong synchronization, in which all interneurons fire each period, and weak synchronization (Brunel and Hakim, 1999), in which interneurons can skip cycles. Strong synchronization is only moderately robust against neuronal heterogeneity (Wang and Buzsáki, 1996), noise (Tiesinga et al., 1998), and sparse connectivity (Wang and Buzsáki, 1996; Hansel and Golomb, 2000). Weak synchronization is more robust, provides a periodic inhibitory drive, and has a potentially larger information capacity (Tiesinga and José, 2000b). Robustness of gamma oscillations when pyramidal cells also project to the interneurons, γ-II, has not yet been investigated in full detail, but see Ermentrout and Kopell (1998) and Kopell et al. (2000). The simulations presented here show that these oscillations are not necessarily stable (Zhang et al., 2000). Instead, stability depends critically on the quantitative properties of the synaptic connections and intrinsic properties (such as driving current).

A number of papers addressed the generation of theta rhythms in the hippocampus using biophysical models (Traub et al., 1992; Liljenstrom and Hasselmo, 1995; Wallenstein and Hasselmo, 1997a,b; Menschik and Finkel, 1998, 1999). Traub et al. (1992) found carbachol-induced theta-frequency oscillations in a model of the CA3 region of hippocampus. Their model pyramidal cell did not contain an I_M current, and final bursts during the theta cycle. Pyramidal cells did not burst during CCH-θ in our simulations and experiments. In our simulations, I_M is important in driving the transition from asynchronous CCH-θ to CCH-δ. However, an increase in any depolarizing current, or a decrease in a hyperpolarizing current (as was the case here with I_M), can in principle induce this transition in our model. In their model, the frequency of the theta oscillation was determined by $g_{K\text{-}AHP}$ (in Liljenstrom and Hasselmo (1995), a similar role for $I_{K\text{-}AHP}$ was proposed) and the strength of recurrent excitation. When they included fast GABAergic inhibition in the model, a different oscillation was obtained. Individual pyramidal cells fired only during a few cycles, whereas the interneurons fired many spikes between the pyramidal cell population discharges.

In another computational study (Wallenstein and Hasselmo, 1997a), it was found that acetylcholine can cause a transition from a partially synchronized to a globally synchronized state similar to CCH-δ. The theta rhythm there, and in other models, is generated via an externally imposed septohippocampal drive, either in the form of a square wave current at 5 Hz (Menschik and Finkel, 1998, 1999), or a 5-Hz modulation of a leak-conductance together with barrages of fast GABAergic IPSPs (Wallenstein and Hasselmo, 1997a,b). In comparison, the theta-frequency-range oscillations are generated intrinsically in our model network and in in vitro experiments (Fellous and Sejnowski, 2000). The model neuron, as in experimental recordings, had a peak in its transfer function and spiked at the top of the depolarization. Furthermore, the model neuron also spiked regularly at theta frequencies upon depolarization. The model neuron explained the seemingly paradoxical experimental finding that delta-frequency-range oscillations occurred between asynchronous and synchronous oscillations in the theta-frequency-range.

There are other mechanisms that in principle could give rise to theta oscillations. Recently, subthreshold membrane potential oscillations were found in interneurons near the border between the stratum radiatum and stratum lacunosum-moleculare of the rat hippocampus (Chapman and Lacaille, 1999a). These neurons were able to pace CA1 pyramidal cells at theta frequencies (Chap-

man and Lacaille, 1999b). Two distinct $GABA_A$ IPSPs have been found, a fast one and slow one (Banks et al., 1998). The fast IPSP is important in gamma rhythms, whereas the slow IPSP has a time-scale similar to that of theta rhythms and could, therefore, be involved in theta oscillations (White et al., 2000). In our preparation CCH-θ persists in CA3 in the absence of GABAergic inhibition, indicating that these alternate mechanisms may not be the most important ones for in vitro CCH oscillations.

Synchronous population bursts have been observed in many models, ranging from abstract (Pham et al., 1998) to more biophysical models (Traub and Miles, 1991; Grobler et al., 1998; Barna et al., 1998; Butera et al., 1999b). The basic mechanism is the same as in our model. The spikes or bursts of a few pyramidal cells recruit other cells in a runaway process; the recruitment is then terminated by slow intrinsic currents, synaptic depression, or refractory periods. Little is known about the underlying quantitative intrinsic and network properties. However, a number of basic questions can be addressed by the analysis of long trains of population bursts. A burst can be initiated by a neuron, or group of neurons that always fire earlier than the rest, or are simply more excitable. In that case the interval between consecutive bursts is constant. On the other hand, if a population burst is initiated by noise-induced spiking, then the interburst intervals are stochastic. In that case the noise level and the required number of neurons for burst initiation can be determined from the distribution of interburst intervals. The initial increase of activity during the population bursts yields the probability of successful propagation of presynaptic activity, given anatomical estimates of single-cell connectivity; and the duration of the population burst yields information about the size and connectivity of the pool of neurons that can be recruited by a population burst.

A network state where all three oscillations were present was induced by the presence of inhibition. Interestingly, Williams and Kauer (1997) reported that theta oscillations occurred in regularly spaced bursts (about 20 s). However, blocking fast inhibition abolished the regular interval between bursts, while the theta rhythm remained. It remains to be determined whether the results of our simulations are related to their findings.

Carbachol-induced functional changes and oscillatory regimes

The functional implications of CCH-induced cellular changes are uncertain. Hasselmo (1995) and Wallenstein and Hasselmo (1997a) proposed that CCH can act as a switch between recall dynamics (for low CCH levels) to learning dynamics (for high CCH levels). For low CCH levels, the attractors of the recurrent network dominate. In contrast, higher CCH levels suppress the feedback excitation in CA3 and thus prevents the previous learned states from dominating the network dynamics. Menschik and Finkel (1998, 1999) suggest that reducing CCH inhibits recall. Reducing CCH levels increases the length of the gamma cycle, reducing the number of cycles available during one theta cycle to relax to an attractor state, and concomitantly the recall becomes less effective. We have shown that in vitro, CCH application can cause transitions between oscillations in different frequency ranges. Similar transitions occur in vivo, though less is known about the mechanisms. What are the consequences of these transitions for network properties, such as the ability to store inputs in attractor states and transmit information? Most of these issues have not yet been addressed in large-scale simulations. However, the results presented here serve as the basis for future experimental and model investigations into the nature of hippocampal rhythms.

Acknowledgments

Some of the numerical calculations were performed at the High Performance Computer Center at Northeastern University. The work was supported by the Sloan Center for Theoretical Neurobiology at the Salk Institute, and the Center for Interdisciplinary Research on Complex Systems at Northeastern University. We thank Shuang Zhang and John Lisman for their contributions in the preliminary stages of this work. We also thank the two anonymous referees for their suggestions, which have helped improve our paper significantly.

REFERENCES

Alonso A, Llinas R. 1989. Subthreshold Na+-dependent theta-like rhythmicity in stellate cells of entorhinal cortex layer II. Nature 342:175–177.

Arfken G, Weber H. 1995. Mathematical methods for physicists. San Diego: Academic Press.

Banks M, Li T, Pearce R. 1998. The synaptic basis of $GABA_A$, slow. J Neurosci 15:1305–1317.

Barna G, Grobler T, Erdi P. 1998. Statistical model of the hippocampal CA3 region II. The population framework: model of rhythmic activity in the CA3 slice. Biol Cybern 79:309–321.

Basar E, Basar-Eroglu C, Karakas S, Schurmann M. 1999. Are cognitive processes manifested in event-related gamma, alpha, theta and delta oscillations in the EEG? Neurosci Lett 259:165–168.

Basar-Eroglu C, Basar E, Demiralp T, Schurmann M. 1992. P300-response: possible psychophysiological correlates in delta and theta frequency channels. A review. Int J Psychophysiol 13:161–179.

Benson D, Blitzer R, Landau E. 1988. An analysis of the depolarization produced in guinea-pig hippocampus by cholinergic receptor stimulation. J Physiol (Lond) 404:479–496.

Bland B, Colom L. 1993. Extrinsic and intrinsic properties underlying oscillation and synchrony in limbic cortex. Prog Neurobiol 41:157–208.

Bland B, Colom L, Konopacki J, Roth S. 1988. Intracellular records of carbachol-induced theta rhythm in hippocampal slices. Brain Res 447: 364–368.

Boguszewicz J, Skrajny B, Kohli J, Roth S. 1996. Evidence that GABA, serotonin, and norepinephrine are involved in the modulation of in vitro rhythmical activity in rat hippocampal slices. Can J Physiol Pharmacol 74:1322–1326.

Bragin A, Jandó G, Nádasdy Z, Hetke J, Wise K, Buzsáki G. 1995. Gamma (40–100 Hz) oscillation in the hippocampus of the behaving rat. J Neurosci 15:47–60.

Brazhnik E, Fox S. 1997. Intracellular recordings from medial septal neurons during hippocampal theta rhythm. Exp Brain Res 114:442–452.

Brazhnik E, Vinogradova O, Stafekhina V, Kitchigina V. 1993. Acetylcholine, theta-rhythm and activity of hippocampal neurons in the rabbit—I. Spontaneous activity. Neuroscience 53:961–970.

Brown D, Adams P. 1980. Muscarinic suppression of a novel voltage-sensitive K+ current in a vertebrate neurone. Nature 283:673–676.
Brunel N, Hakim V. 1999. Fast global oscillations in networks of integrate-and-fire neurons with low firing rates. Neural Comput 11:1621–1671.
Buhl E, Cobb S, Halasy K, Somogyi P. 1995. Properties of unitary IPSPs evoked by anatomically identified basket cells in the rat hippocampus. Eur J Neurosci 7:1989–2004.
Butera R, Rinzel J, Smith J. 1999a. Models of respiratory rhythm generation in the pre-Botzinger complex. I. Bursting pacemaker neurons. J Neurophysiol 82:382–397.
Butera R, Rinzel J, Smith J. 1999b. Models of respiratory rhythm generation in the pre-Botzinger complex. II. Populations of coupled pacemaker neurons. J Neurophysiol 82:398–415.
Chapman C, Lacaille J. 1999a. Cholinergic induction of theta-frequency oscillations in hippocampal inhibitory interneurons and pacing of pyramidal cell firing. J Neurosci 19:8637–8645.
Chapman C, Lacaille J. 1999b. Intrinsic theta-frequency membrane potential oscillations in hippocampal CA1 interneurons of stratum lacunosum-moleculare. J Neurophysiol 81:1296–1307.
Chow C, White J, Ritt J, Kopell N. 1998. Frequency control in synchronized networks of inhibitory neurons. J Comput Neurosci 5:407–420.
Cole A, Nicoll R. 1983. Acetylcholine mediates a slow synaptic potential in hippocampal pyramidal cells. Science 221:1299–1301.
Cole A, Nicoll R. 1984a. Characterization of a slow cholinergic postsynaptic potential recorded in vitro from rat hippocampal pyramidal cells. J Physiol (Lond) 352:173–188.
Cole A, Nicoll R. 1984b. The pharmacology of cholinergic excitatory responses in hippocampal pyramidal cells. Brain Res 305:283–290.
Denk W, Delaney K, Gelperin A, Kleinfeld D, Strowbridge B, Tank D, Yuste R. 1994. Anatomical and functional imaging of neurons using 2-photon laser scanning microscopy. J Neurosci Methods 54:151–162.
Ermentrout G, Kopell N. 1998. Fine structure of neural spiking and synchronization in the presence of conduction delays. Proc Natl Acad Sci USA 95:1259–1264.
Fellous J-M, Sejnowski T. 2000. Cholinergic induction of oscillations in the hippocampal slice in the slow (0.5–2 Hz), theta (5–12 Hz), and gamma (35–70 Hz) bands. Hippocampus 10:187–197.
Fellous J-M, Johnston T, Segal M, Lisman J. 1998. Carbachol-Induced rhythms in the hippocampal slice: slow (0.5–2 Hz), theta (4–10 Hz) and gamma (80–100 Hz) oscillations. In: Bower J, editor. Computational neuroscience. New York: Plenum Press. p 367–372.
Fellous J-M, Rao R, Houweling A, Sejinowski T. 1999. Spike timing reliability in the prefrontal cortex depends on the frequency content of its synaptic inputs. Society for Neuroscience Abstracts 25:885.
Fisahn A, Pike F, Buhl E, Paulsen O. 1998. Cholinergic induction of network oscillations at 40 Hz in the hippocampus in vitro. Nature 394:186–189.
Fischer Y, Gahwiler B, Thompson S. 1999. Activation of intrinsic hippocampal theta oscillations by acetylcholine in rat septo-hippocampal cocultures. J Physiol [Lond] 519:405–413.
Freund T, Antal M. 1988. GABA-containing neurons in the septum control inhibitory interneurons in the hippocampus. Nature 336:170–173.
Freund T, Buzsaki G. 1996. Interneurons of the hippocampus. Hippocampus 6:347–470.
Frotscher M, Leranth C. 1985. Cholinergic innervation of the rat hippocampus as revealed by choline acetyltransferase immunocytochemistry: a combined light and electron microscopic study. J Comp Neurol 239:237–246.
Gahwiler B, Brown D. 1987. Muscarine affects calcium-currents in rat hippocampal pyramidal cells in vitro. Neurosci Lett 76:301–306.
Glass A, Riding R. 1999. EEG differences and cognitive style. Biol Psychol 51:23–41.
Grobler T, Barna G, Erdi P. 1998. Statistical model of the hippocampal CA3 region. I. The single-cell module: bursting model of the pyramidal cell. Biol Cybern 79:301–308.
Halliwell J, Adams P. 1982. Voltage-clamp analysis of muscarinic excitation in hippocampal neurons. Brain Res 250:71–92.
Hansel D, Golomb D. 2000. The number of synaptic inputs and the synchrony of large sparse neuronal networks. Neural Comput 12:1095–1139.
Hasselmo M. 1995. Neuromodulation and cortical function: modeling the physiological basis of behavior. Behav Brain Res 67:1–27.
Hasselmo M, Schnell E. 1994. Laminar selectivity of the cholinergic suppression of synaptic transmission in rat hippocampal region CA1: computational modeling and brain slice physiology. J Neurosci 14:3898–3914.
Hasselmo M, Schnell E, Barkai E. 1995. Dynamics of learning and recall at excitatory recurrent synapses and cholinergic modulation in rat hippocampal region CA3. J Neurosci 15:5249–5262.
Hines M, Carnevale N. 1997. The NEURON simulation environment. Neural Comput 9:1179–1209.
Hutcheon B, Miura R, Puil E. 1996a. Models of subthreshold membrane resonance in neocortical neurons. J Neurophysiol 74:698–714.
Hutcheon B, Miura R, Puil E. 1996b. Subthreshold membrane resonance in neocortical neurons. J Neurophysiol 74:683–697.
Koch C. 1999. Biophysics of computation. New York: Oxford University Press.
Kocsis B, Bragin A, Buzsáki G. 1999. Interdependence of multiple theta generators in the hippocampus: a partial coherence analysis. J Neurosci 19:6400–6412.
Konopacki J, MacIver M, Bland B, Roth S. 1987. Carbachol-induced EEG "theta" activity in hippocampal brain slices. Brain Res 405:196–198.
Kopell N, Ermentrout G, Whittington M, Traub R. 2000. Gamma rhythms and beta rhythms have different synchronization properties. Proc Natl Acad Sci USA 97:1867–1872.
Lampl I, Yarom Y. 1997. Subthreshold oscillations and resonant behavior: two manifestations of the same mechanism. Neuroscience 87:325–341.
Lee M, Chrobak J, Sik A, Wiley R, Buzsaki G. 1994. Hippocampal theta activity following selective lesion of the septal cholinergic system. Neuroscience 62:1033–1047.
Leung L. 1998. Generation of theta and gamma rhythms in the hippocampus. Neurosci Biobehav Rev 22:275–290.
Leung L, Yim C. 1991. Intrinsic membrane potential oscillations in hippocampal neurons in vitro. Brain Res 553:261–274.
Leung L, Yu H. 1998. Theta-frequency resonance in hippocampal CA1 neurons in vitro demonstrated by sinusoidal current injection. J Neurophysiol 79:1592–1596.
Liljenstrom H, Hasselmo M. 1995. Cholinergic modulation of cortical oscillatory dynamics. J Neurophysiol 74:288–297.
Llinas R, Grace A, Yarom Y. 1991. In vitro neurons in mammalian cortical layer 4 exhibit intrinsic oscillatory activity in the 10- to 50-Hz frequency range. Proc Natl Acad Sci USA 88:897–901.
MacVicar B, Tse F. 1989. Local neuronal circuitry underlying cholinergic rhythmical slow activity in CA3 area of rat hippocampal slice. J Physiol (Lond) 417:197–212.
Madison D, Lancaster B, Nicoll R. 1987. Voltage clamp analysis of cholinergic action in the hippocampus. J Neurosci 7:733–741.
Mainen Z, Sejnowski T. 1994. Influence of dendritic structure on firing pattern in model neocortical neurons. Nature 383:363–366.
Makeig S, Jung T. 1996. Tonic, phasic, and transient EEG correlates of auditory awareness in drowsiness. Brain Res Cogn Brain Res 4:15–25.
Marrosu F, Portas C, Mascia M, Casu M, Fa M, Giagheddu M, Imperato A, Gessa G. 1995. Microdialysis measurement of cortical and hippocampal acetylcholine release during sleep-wake cycle in freely moving cats. Eur J Neurosci 7:358–366.
McCormick D. 1989. Cholinergic and noradrenergic modulation of thalamocortical processing. Trends Neurosci 12:215–221.

McCormick D. 1992. Neurotransmitter actions in the thalamus and cerebral cortex and their role in neuromodulation of thalamocortical activity. Prog Neurobiol 39:337–388.
Menschik E, Finkel L. 1998. Neuromodulatory control of hippocampal function: towards a model of Alzheimer's disease. Artif Intell Med 13:99–121.
Menschik E, Finkel L. 1999. Cholinergic neuromodulation and Alzheimer's disease: from single cells to network simulations. Prog Brain Res 121:19–45.
Migliore M, Cook E, Jaffe D, Turner D, Johnston D. 1995. Computer simulations of morphologically reconstructed CA3 hippocampal neurons. J Neurophysiol 73:1157–1168.
Nakajima Y, Nakajima S, Leonard R, Yamaguchi K. 1986. Acetylcholine raises excitability by inhibiting the fast transient potassium current in cultured hippocampal neurons. Proc Natl Acad Sci USA 83:3022–3026.
Patil M, Hasselmo M. 1999. Modulation of inhibitory synaptic potentials in the piriform cortex. J Neurophysiol 81:2103–2118.
Perkel D, Mulloney B, Rudelli RW. 1981. Quantitative methods for predicting neuronal behavior. Neuroscience 56:823–827.
Peterlin Z, Kozloski J, Mao B, Tsiola A, Yuste R. 2000. Optical probing of neuronal circuits with calcium indicators. Proc Natl Acad Sci USA 97:3619–3624.
Pham J, Pakdaman K, Vibert J-F. 1998. Noise-induced coherent oscillations in randomly connected neural networks. Physical Review E 58: 3610–3622.
Pinsky P, Rinzel J. 1994. Intrinsic and network rhythmogenesis in a reduced Traub model for CA3 neurons. J Comput Neurosci 1:39–60.
Press W, Teukolsky S, Vetterling WT, Flannery BP. 1992. Numerical recipes. Cambridge: Cambridge University Press.
Rieke F, Warland D, de Ruyter van Steveninck RR, Bialek W. 1997. Spikes: exploring the neural code. Cambridge, MA: MIT Press.
Ritz R, Sejnowski T. 1997. Synchronous oscillatory activity in sensory systems: new vistas on mechanisms. Curr Opin Neurobiol 7:536–546.
Sheridan R, Sutor B. 1990. Presynaptic M1 muscarinic cholinoceptors mediate inhibition of excitatory synaptic transmission in the hippocampus in vitro. Neurosci Lett 108:273–278.
Singer W, Gray C. 1995. Visual feature integration and the temporal correlation hypothesis. Annu Rev Neurosci 18:555–586.
Soltesz I, Deschenes M. 1993. Low- and high-frequency membrane potential oscillations during theta activity in CA1 and CA3 pyramidal neurons of the rat hippocampus under ketamine-xylazine anesthesia. J Neurophysiol 70:97–116.
Steriade M, Amzica F, Nunez A. 1993. Cholinergic and noradrenergic modulation of the slow (approximately 0.3 Hz) oscillation in neocortical cells. J Neurophysiol 70:1385–1400.
Stewart M, Fox S. 1990. Do septal neurons pace the hippocampal theta rhythm? Trends Neurosci 13:163–168.
Tiesinga P, José J. 2000a. Robust gamma oscillations in networks of inhibitory hippocampal interneurons. Network 11:1–23.
Tiesinga P, José J. 2000b. Synchronous clusters in a noisy inhibitory network. J Comput Neurosci 9:49–65.
Tiesinga P, Rappel W-J, José J. 1998. Synchronization in networks of noisy interneurons. In: Bower J, editor. Computational Neuroscience. New York: Plenum Press. p 555–559.
Traub R, Miles R. 1991. Neuronal networks of the hippocampus. Cambridge: Cambridge University Press.
Traub R, Wong R, Miles R, Michelson H. 1991. A model of a CA3 hippocampal pyramidal neuron incorporating voltage-clamp data on intrinsic conductances. J Neurophysiol 66:635–650.
Traub R, Miles R, Buzsáki G. 1992. Computer simulations of carbachol-driven rhythmic population oscillations in the CA3 region of the in vitro rat hippocampus. J Physiol [Lond] 451:653–672.
Traub R, Whittington M, Colling S, Buzsaki G, Jeffreys J. 1996a. Analysis of gamma rhythms in the rat hippocampus in vitro and in vivo. J Physiol [Lond] 493:471–484.
Traub R, Whittington M, Stanford I, Jeffreys J. 1996b. A mechanism for generation of long-range synchronous fast oscillations in the cortex. Nature 383:621–624.
Vinogradova O. 1995. Expression, control, and probable functional significance of the neuronal theta-rhythm. Prog Neurobiol 45:523–583.
Wallenstein G, Hasselmo M. 1997a. Functional transitions between epileptiform-like activity and associative memory in hippocampal region CA3. Brain Res Bull 43:485–493.
Wallenstein G, Hasselmo M. 1997b. GABAergic modulation of hippocampal population activity: sequence learning, place field development, and the phase precession effect. J Neurophysiol 78:398–408.
Wang X-J, Buzsáki G. 1996. Gamma oscillation by synaptic inhibition in a hippocampal interneuronal network model. J Neurosci 16:6402–6413.
Wang X-J, Rinzel J. 1993. Spindle rhythmicity in the reticularis thalami nucleus: synchronization among mutually inhibitory neurons. Neuroscience 53:899–904.
Warman E, Durand D, Yuen G. 1994. Reconstruction of hippocampal CA1 pyramidal cell electrophysiology by computer simulation. J Neurophysiol 71:2033–2045.
White J, Budde T, Kay A. 1995. A bifurcation analysis of neuronal subthreshold oscillations. Biophys J 69:1203–1217.
White J, Chow C, Ritt J, Soto-Treviño C, Kopell N. 1998a. Synchronization and oscillatory dynamics in heterogeneous, mutually inhibited neurons. J Comput Neurosci 5:5–16.
White J, Klink R, Alonso A, Kay A. 1998b. Noise from voltage-gated ion channels may influence neuronal dynamics in the entorhinal cortex. J Neurophysiol 80:262–269.
White J, Banks M, Pearce R, Kopell N. 2000. Networks of interneurons with fast and slow gamma-aminobutyric acid type A (GABAA) kinetics provide substrate for mixed gamma-theta rhythm. Proc Natl Acad Sci USA 97:8128–8133.
Whittington M, Traub R, Jeffreys J. 1995. Synchronized oscillations in interneuron networks driven by metabotropic glutamate receptor activation. Nature 373:612–615.
Williams J, Kauer J. 1997. Properties of carbachol-induced oscillatory activity in rat hippocampus. J Neurophysiol 78:2631–2640.
Ylinen A, Soltesz I, Bragin A, Penttonen M, Sik A, Buzsaki G. 1995. Intracellular correlates of hippocampal theta rhythm in identified pyramidal cells, granule cells, and basket cells. Hippocampus 5:78–90.
Zhang S, Tiesinga P, José J. 2000. Model of carbachol-induced gamma-frequency oscillations in hippocampus. Neurocomputing 32–33:617–622.

APPENDIX

Pyramidal Cell Model

The Pinsky-Rinzel model (Pinsky and Rinzel, 1994) consists of a somatic compartment with membrane potential V_s, and a dendritic compartment with membrane potential V_d. The membrane potentials satisfy the following dynamics:

$$C_m \frac{dV_s}{dt} = -g_L(V_s - E_L) - I_{Na} - I_{K\text{-}DR} + \frac{1}{2} g_c(V_d - V_s),$$

$$C_m \frac{dV_d}{dt} = -g_L(V_d - E_L) - I_{Ca} - I_{K\text{-}AHP} - I_{K\text{-}C} - I_M - I_{NaO} - I_{KO} - I_{syn,e} + \frac{1}{2} g_c(V_s - V_d) + I_{app} \quad (1)$$

with the currents given by

$$I_{Na} = g_{Na} m_\infty^2(V_s) h (V_s - E_{Na}),$$
$$I_{K\text{-}DR} = g_{K-DR} n (V_s - E_K),$$
$$I_{Ca} = g_{Ca} s^2 (V_d - E_{Ca}),$$
$$I_{K\text{-}C} = g_{K-C} c \min(Ca/250, 1)(V_d - E_K),$$
$$I_{K\text{-}AHP} = g_{K-AHP} q (V_d - E_K),$$
$$I_M = g_M r^2 (V_d - E_K),$$
$$I_{KO} = g_{KO} a (V_d - E_K),$$
$$I_{NaO} = g_{NaO} b (V_d - E_{Na}).$$

The synaptic current $I_{syn,e}$ is defined below. The calcium concentration Ca satisfied the following first-order equation

$$\frac{dCa}{dt} = -0.13 I_{Ca} - 0.075 Ca \tag{2}$$

whereas the kinetic variables satisfied the following first-order kinetics

$$\frac{dx}{dt} = \phi(\alpha_x(1 - x) - \beta_x x). \tag{3}$$

Here x labels the different kinetic variables h, n, m, s, c, q, r, a, and b, and ϕ is a dimensionless time-scale that was used to tune the rate with which the channels open or close.

$$\alpha_m = \frac{0.32(-46.9 - V_s)}{\exp((-46.9 - V_s)/4) - 1}$$
$$\beta_m = \frac{0.28(V_s + 19.9)}{\exp((V_s + 19.9)/5) - 1}$$
$$\alpha_n = \frac{0.016(-24.9 - V_s)}{\exp((-24.9 - V_s)/5) - 1}$$
$$\beta_n = 0.25 \exp(-1 - 0.025 V_s)$$
$$\alpha_h = 0.128 \exp((-43 - V_s)/18)$$
$$\beta_h = \frac{4}{1 + \exp((-20 - V_s)/5)}$$
$$\alpha_s = \frac{1.6}{1 + \exp(-0.072(V_d - 5))}$$
$$\beta_s = \frac{0.02(V_d + 8.9)}{\exp((V_d + 8.9)/5) - 1}$$
$$\alpha_r = 0.016 \exp((V_d + 52.7)/23)$$
$$\beta_r = 0.016 \exp(-(V_d + 52.7)/18.8)$$
$$\alpha_q = 0.01 \min(Ca/500, 1)$$
$$\beta_q = 1/t_{K\text{-}AHP}$$
$$a_\infty = \frac{1}{1 + \exp(-(V_d + 63)/10)}$$
$$\tau_a = 30$$
$$b_\infty = \frac{1}{1 + \exp(-(V_d + 60)/5)}$$
$$\tau_b = 0.05$$
$$\alpha_c = \frac{\exp((V_d + 50)/11) - \exp((V_d + 53.5)/27)}{18.975} \quad V_d \le -10$$
$$= 2 \exp((V_d + 53.5)/27) \quad V_d > -10$$
$$\beta_c = 2 \exp((V_d + 53.5)/27) - \alpha_c \quad V_d \le -10$$
$$= 0 \quad V_d > -10.$$

We used the following standard set of parameter values for the pyramidal cell. Reversal potentials were $E_{Na} = 60$, $E_{Ca} = 80$, $E_K = -75$, and $E_L = -60$ mV. Dimensionless time-scale was $\phi = 1$, and $t_{K-AHP} = 1{,}000$ ms (except in Fig. 9a). The conductances were $g_c = 2.1$, $g_{Na} = 30$, $g_{K\text{-}DR} = 15$, $g_L = 0.1$, $g_{Ca} = 10$, $g_{K\text{-}AHP} = 0.8$, $g_{K\text{-}C} = 15$, $g_M = 0.4$, $g_{KO} = 0.625$, and $g_{NaO} = 0.075$ mS/cm^2. Injected current $I_{app} = 0.0$. Capacitance $C_m = 3$ μF/cm^2.

Hippocampal Interneuron

The Wang-Buzsáki model neuron (Wang and Buzsáki, 1996) consisted of a single compartment, with the following equation for the membrane potential

$$C_m \frac{dV}{dt} = -I_{Na} - I_K - I_L - I_{syn,i} + I_{int} \tag{4}$$

with the currents given by

$$I_L = g_L(V - E_L),$$
$$I_{Na} = g_{Na} m_\infty^3(V) h (V - E_{Na}),$$
$$I_K = g_K n^4 (V - E_K).$$

The kinetic variables h and n satisfied Eq. 3 as above. The rate constants were (Wang and Buzsáki, 1996):

$$\alpha_m = \frac{-0.1(V + 35)}{\exp(-0.1(V + 35)) - 1},$$
$$\beta_m = 4 \exp(-(V + 60)/18),$$
$$\alpha_h = 0.07 \exp(-(V + 58)/20),$$
$$\beta_h = \frac{1}{\exp(-0.1(V + 28)) + 1},$$
$$\alpha_n = \frac{-0.01(V + 34)}{\exp(-0.1(V + 34)) - 1},$$
$$\beta_n = 0.125 \exp(-(V + 44)/80).$$

The kinetic variable m was approximated by its asymptotic value $m_\infty(V(t)) = \alpha_m/(\alpha_m + \beta_m)$ instantaneously (Wang and Buzsáki, 1996).

The standard set of values for the interneuron conductances used here was $g_{Na} = 35$, $g_K = 9$, and $g_L = 0.1$ (in mS/cm^2), and $E_{Na} = 55$, $E_K = -90$, and $E_L = -65$ mV. The membrane capacitance was $C_m = 1$ μF/cm^2. Unless noted differently, $I_{int} = 1$ μA/cm^2. The isolated interneuron network spiked at approximately 39 Hz (Wang and Buzsáki, 1996; Tiesinga et al., 1998).

Synaptic Connections

The synaptic currents $I_{syn,e}$ in Eq. 1 and $I_{syn,i}$ in Eq. 4 were given by the following expression:

$$I_{syn,e} = g_{AMPA}(e \rightarrow e)(V - E_{AMPA}) \sum_j c_{kj}^{e \rightarrow e} s_j^e + g_{GABA}(i \rightarrow e) \times (V - E_{GABA}) \sum_j c_{kj}^{i \rightarrow e} s_j^i$$

$$I_{syn,i} = g_{AMPA}(e \rightarrow i)(V - E_{AMPA}) \sum_j c_{kj}^{e \rightarrow i} s_j^e + g_{GABA}(i \rightarrow i) \times (V - E_{GABA}) \sum_j c_{kj}^{i \rightarrow i} s_j^i.$$

Here V is the membrane potential of the postsynaptic neuron with index k (Eqs. 1 and 4). The pyramidal cells are labeled by e, and the interneurons by i. s_j^e (s_j^i) is the kinetic variable labeled by the index j of the presynaptic neuron, $c_{kj}^{x \rightarrow y} = 1$ if there was a connection between presynaptic neuron j and postsynaptic neuron k, and zero otherwise. The connectivity matrix $c_{kj}^{x \rightarrow y}$ was calculated at the start of the run. For all possible connections $j \rightarrow k$ we drew a random number ξ that was uniformly distributed between 0 and 1, then $c_{kj}^{x \rightarrow y} = 1$ if $\xi \leq P(x \rightarrow y)$, and zero otherwise. The connection matrices were determined for all four combinations of $x = i, e$, and $y = i, e$. For certain simulation runs we divided the pyramidal cell population into two groups, e_w and e_s, or three groups, e_s, e_{w1}, and e_{w2}. The same formalism also applied to the synaptic connections between these groups.

The synaptic gating variable s_e for the AMPA synapses satisfied (with the neuron index suppressed):

$$\frac{ds_e}{dt} = H(V_{pre} + 40)(1 - s_e) - \beta_e s_e. \quad (5)$$

Here H is the Heaviside function, $H(x) = 1, x > 0$, and $H(x) = 0, x < 0$, $\beta_e = 0.5\ \text{ms}^{-1}$ is the decay rate.

The synaptic gating variable s_i for the $GABA_A$ synapse obeyed the following equation (Perkel et al., 1981; Wang and Rinzel, 1993; Wang and Buzsáki, 1996):

$$\frac{ds_i}{dt} = \alpha_i F(V_{pre})(1 - s_i) - \beta_i s_i \quad (6)$$

with $\alpha_i = 12\ \text{ms}^{-1}$, $\beta_i = 1/t_{GABA,i \rightarrow i}$ for mutual inhibition, and $\beta_i = 1/t_{GABA,i \rightarrow e}$ for the inhibitory projection to pyramidal cells, $F(V_{pre}) = 1/(\exp(-V_{pre}/2) + 1)$, and V_{pre} is the presynaptic potential. The function $F(V_{pre})$ was chosen such that when the presynaptic neuron fired, $V_{pre} > 0$, the synaptic channel opened. We took $t_{GABA,i \rightarrow i} = t_{GABA,i \rightarrow e} = 10$ ms, except in Figure 9c. We used a reversal potential of $E_{GABA} = -75$ mV for $GABA_A$ synapses (Buhl et al., 1995), and $E_{AMPA} = 0$ mV for AMPA synapses.